Micropatterned Fibrin Hydrogels for Increased Cardiomyocyte Alignment

A thesis to be submitted to the faculty of Worcester Polytechnic Institute in partial fulfillment of the requirements for the Degree of Master of Science.

November 13, 2019

Submitted by:

Elizabeth Jane English
Department of Biomedical Engineering

Approved by:

George D. Pins, PhD, Advisor
Professor
Department of Biomedical Engineering

Jeannine M. Coburn, PhD, Chair
Assistant Professor
Department of Biomedical Engineering

Glenn R. Gaudette, PhD
Professor
Department of Biomedical Engineering

Acknowledgments

I want to thank every person who helped contribute to this research because this thesis was on the verge of collapse many times. This includes most of the Gateway community's support but an extra shout out to the members of the Gaudette Lab and Coburn Lab for their scientific expertise. Special thanks to:

- Katrina Hansen, PhD
- Emily Robbins
- Kimberly Ornell, PhD
- Alycia Abbott
- Natalia Vargas Montoya
- Nhi Phan
- Dalia Shendi, PhD
- Jonian Grosha
- Emily Caron
- Eric Larsen
- Katherine Pearce
- Joshua Harvey, PhD

Thank you to my committee member Glenn Gaudette, PhD, my committee chair Jeannine Coburn, PhD, and my thesis advisor George Pins, PhD for lending their knowledge, expertise, patience, and time to help me complete a thesis we can all be proud of. Special thanks to George Pins for helping me grow scientifically despite my perpetual bad attitude.

I also want to thank the past and present members of the Pins Lab with a special thanks to former member Megan Chrobak, PhD for her help in transitioning the project to me. Additionally, I'd like to thank Meagan Carnes for being there for me throughout this research journey. You're almost free, too.

I would like to acknowledge the former members of the Marchese Lab at MCW – Olga Alekhina, Natalie Ward, Mudassir Ali, James Buhrmaster, and Sarah Mahn, among others – who encouraged me to go back to school and have always been an excellent network of support for me. I'm so proud of all of us and the new lives we've created for ourselves.

And of course, thank you to my friends and family for their support as I skipped town (again) and started over in Worcester. Shout out to my mom Susan Jacobson and oldest friend Ana Marija Fonceva for handling the bulk of this stress with me. After 2+ years of shared misery, all you get is this shared dedication.

Abstract

Cardiovascular disease is the leading cause of death in the US, which can result in blockage of a coronary artery, triggering a myocardial infarction (MI). After a MI, hypoxic ventricular myocardial tissue dies, resulting in the deposition of non-contractile scar tissue and remodeling of the ventricle, leading to decreased cardiac output and ultimately heart failure. Currently, the gold-standard solution for total heart failure is a heart transplant. As donor hearts are in short supply, an alternative to total-organ transplantation is surgically remodeling the ventricle with the implantation of a cardiac patch. Acellular cardiac patches have previously been investigated using synthetic or decellularized native materials in effort to improve cardiac function. However, a limitation of this strategy is that acellular cardiac patches only reshape the ventricle and do not increase cardiac contractile function. By incorporating the use of a clinically relevant cell type and by matching native architecture, we propose the use of a highly aligned fibrin scaffold to support the maturation of human induced pluripotent stem cell cardiomyocytes (hiPS-CM) for use as a cell-populated cardiac patch. By micropatterning fibrin hydrogels, hiPS-CM seeded on the surface of this scaffold become highly aligned, which is crucial for increased contractile output. Our lab previously developed a composite fibrin hydrogel and microthread cardiac patch matching mechanical properties of native myocardium. By micropatterning fibrin hydrogel alone, we were able to match cellular alignment of hiPS-CM to that of native myocardium. hiPS-CMs seeded on this surface were found to express distinct sarcomere alignment and circumferential connexin-43 staining at 14 days of culture as well as cellular elongation, which are necessary for mature contractile properties. Constructs were also cultured under electrical stimulation to promote increased contractile properties. After 7 days of stimulation, contractile strains of micropatterned constructs were significantly higher than unpatterned controls. These results suggest that the use of topographical cues on fibrin scaffolds may be a promising strategy for creating engineered myocardial tissue to repair damaged myocardium.

Table of Contents

Table of Figures

Table of Tables

Table of Abbreviations

2D – Two dimensional
3D – Three dimensional
AFM – Atomic force microscopy
ANOVA – Analysis of Variance
CABG – Coronary artery bypass graft
CM – Cardiomyocyte
cm – Centimeter
CVD – Cardiovascular disease
DMEM – Dulbecco's Modified Eagle's Medium
ECM – Extracellular matrix
FBR – Foreign body response
fps – frames per second
HDM – High-density mapping
hES – Human embryonic stem cell
hiPS – Human induced pluripotent stem cell
hiPS-CM - human induced pluripotent stem cell cardiomyocytes
hMSC – Human mesenchymal stem cell
hPS – Human pluripotent stem cell
hr – Hour
ICD – Intercalated discs
IQR – Interquartile Range
kPa – Kilopascal
MI – Myocardial infarction
min – Minute
mL – Milliliter
mm – Millimeter
mM – Millimolar
N – Newton
PBS – Phosphate-buffered saline
PDMS – Polydimethylsiloxane
ROI – Region of interest
rNVM – Rat neonatal ventricular myocyte
sec – Second
SEM – Standard error of the mean
µL – Microliters
µm – Micrometers

Chapter 1 Introduction

Cardiovascular diseases (CVD) are the leading cause of death and affect 48% of adults over the age of 20 in the US [1]. CVD encompasses diseases that lead to damage of heart tissue and often result in a myocardial infarction (MI), which occurs when an obstruction in the coronary arteries prevents oxygen from reaching the myocardium and results in tissue death [1, 2]. After tissue death, cardiac output is diminished as non-contractile scar tissue replaces the tissue due to cardiomyocytes' inability to regenerate and remodel this diseased environment.

The only long-term treatment available for end stage heart failure is whole organ transplant; however, nearly 4,000 people are currently on the waiting list in the US [1]. An alternative therapy can be performed in the form of Surgical Ventricle Restoration (SVR), also known as the Dor procedure, in which damaged myocardium is replaced with a synthetic or decellularized matrix cardiac patch [3]. This procedure removes much of the scar tissue and reshapes the ventricle; however, full functionality is not necessarily restored to the ventricle. This procedure often requires a coronary artery bypass graft (CABG) and mitral valve replacement, all performed during SVR, to ensure a successful cardiac patch implantation. Current commercially available cardiac patches are made from synthetic materials or decellularized tissues [4]. Implantation of these patches have been shown to lead to fibrous encapsulation, granular tissue formation, and poor to no cell infiltration of the area, preventing significant functional recovery of the new tissue [4-6]. Therefore, there is a need for a functional replacement for ventricle myocardium.

Naturally sourced biomaterials have been examined by many groups to create a cell-populated replacement for diseased myocardium [7, 8]. Additionally, by culturing under

electrical or mechanical stimulation, these groups saw an increase in synchronous beating of cells prior to implantation and coupling to host myocardium post implantation. The use of electrical stimulation has also been shown to increase contractile properties and mature cell phenotype in stem cell cardiomyocytes [9]. Based on this knowledge**, we hypothesize that micropatterning fibrin hydrogels for the use of a cardiac patch will increase cardiomyocyte alignment that, along with culturing under electrical stimulation, will promote increased contractile strain compared to unpatterned hydrogel.** The use of an implantable, nonimmunogenic material and autologous cell source in the form of human induced pluripotent stem cell cardiomyocytes (hiPS-CM) could prevent fibrous encapsulation post implantation and allow for a functional, contractile environment of integrated engineered tissue [10, 11]. To accomplish our goal, we divided the hypothesis into three specific aims:

1. Develop fibrin scaffolds with aligned surfaces to increase nuclear orientation.
2. Determine topographic features that maximize hiPS-CM cellular morphology.
3. Characterize the contractile strain response of hiPS-CM seeded micropatterns to electrical stimulation.

Our micropatterned fibrin hydrogel was designed to promote cardiomyocyte alignment through topographical micropatterning in linear, channel geometry. This was accomplished through the use of photolithography to create a polydimethylsiloxane (PDMS) negative replicate which served as a patterned substrate for fibrin hydrogels to conform to the geometries during polymerization. After analyzing the fidelity through ImageJ measurements, the nuclear alignment of cells was confirmed using C2C12 murine skeletal myoblasts. Nuclear alignment of hiPS-CM, an initial verification of nuclear alignment, was

performed before analyzing the phenotype of cell-seeded micropatterned hydrogels. Constructs showed mature sarcomeric alignment and connexin-43 staining and revealed an increase in mature phenotypic expression over a 14-day culture period. Finally, the contractile functionality was measured using a custom pixel-tracking algorithm to determine contractile strain when samples were cultured with and without electrical stimulation. Micropatterned hydrogels displayed increased contractile strains compared to coverslip controls. When cultured under electrical stimulation, micropatterned hydrogels showed an increase in contractile strain compared to both the coverslip and unpatterned control, indicating increased alignment lead to increased contractile properties in addition to electrical stimulation.

The phenotypic and contractile analysis of these hiPS-CM-seeded micropatterned fibrin hydrogels suggest a promising approach to the design of a physiologically relevant cellular cardiac patch. Additional analysis of contractile properties and *in vitro* markers of cellular maturity would be recommended in the short term as well as an eventual analysis of long-term *in vitro* and *in vivo* culture. Ultimately, this micropatterned cardiac patch has the promise of an autologously sourced, functional engineered heart tissue.

Chapter 2 Background

There are currently nearly 4,000 people on the donor waiting list for heart transplantation [1]. As donor hearts are in high demand, alternative procedures have been explored to restore contractile function to the myocardium in end stage heart failure, such as replacement of damaged ventricular tissue post MI through the use of a cardiac patch. This thesis examines the alignment of cardiomyocytes for increased contractile properties on a cardiac patch for tissue engineered left ventricle myocardium. To understand the clinical need, the anatomy of the human heart as it related to the pathology of heart failure is examined, as well as clinical strategies for treating heart disease and related medical devices. Various methods for aligning engineered myocardium are outlined in addition to the limitations of current clinical therapies before examining previous methods explored by our research group and a brief introduction to the materials used to create our next generation of cardiac patch.

2.1 Anatomy and Physiology of the Human Heart

The circuit of blood flow through the human heart is divided into the pulmonary circuit and the systemic circuit [12]. As deoxygenated blood enters the heart, it starts in the right atrium, moving through the tricuspid valve into the right ventricle before being ejected from the heart to the lungs for oxygenation via the pulmonary artery. Oxygenation occurs in the lungs, and the oxygenated blood returns to the heart at the left atrium via the pulmonary vein, completing the pulmonary circuit. This blood is ejected to the left ventricle through the mitral valve where it then travels through the aorta to the rest of the body. Upon returning to the heart deoxygenated, the blood completes the systemic circuit. These structures are outlined in Figure 1A.

The cardiac action potential originates in the right atrium at the pacemaker of the heart, known as the sinoatrial (SA) node, where it spreads through the atria [12]. From there, the excitation travels to the atrioventricular (AV) node, where the conduction is slowed. At this point, the atria contract and the ventricles fill with blood. The excitation next travels to the bundle of His where it is spread through the ventricles via the Purkinje fibers. The Purkinje fibers allow the ventricle cardiomyocytes to contract in a coordinated manner. This electrical pathway is outlined in Figure 1B.

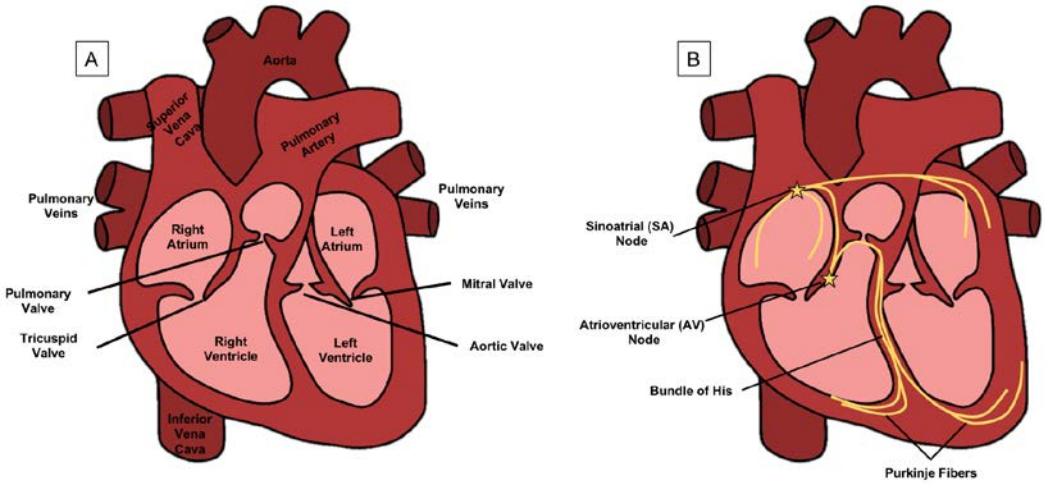

Figure 1 Diagrams of the structures of the heart (A) and the electrical pathway (B).

The atria are low-pressure chambers that function as a reservoir for blood; the ventricles, however, are composed of muscle fibers originating at the base of the heart that run to the apex, forming the epicardium (exterior of ventricle) and eventually twisting inward to form the endocardium (interior of ventricle) and papillary muscles (necessary for preventing inversion of valves) [12]. Between the epicardium and the endocardium lies the muscular layer known as the myocardium. The endocardium and epicardium are ~100 μm thick membranes, while the myocardium is arranged in three to four laminar layers 48.4±20.4 μm thick and are offset at -60˚ to the epicardium ranging to +60˚ to the endocardium [13, 14].

The ventricular myocardium is composed on cardiomyocytes, myeloid cells, fibroblasts, and microvasculature [15]. Cardiomyocytes are the functional unit of the heart, while fibroblasts make up the connective tissue between the cardiomyocytes, myeloid cells, and microvasculature. While it is generally agreed that cardiomyocytes do not proliferate or renew in adult tissue [15, 16], cardiac fibroblasts continue to renew and remodel the extracellular matrix (ECM) [17]. There is, however, a delicate balance between ECM degradation and deposition that must be maintained for proper cardiac function. In the event of cardiomyocyte death, cardiac fibroblasts undergo phenotypic change to become myofibroblast, which are proliferative and increase synthesis of ECM-degrading metalloproteinases (MMPs) and collagen [18]. These proteins are necessary for wound healing, but contractile cardiomyocytes do not return to the area, and the tissue remodels as noncontractile scar tissue with limited cardiac output.

2.1.1 Remodeling of the Left Ventricle in Response to Myocardial Infarction

CVD encompass many diseases that lead to a blocking or narrowing of blood vessels that can lead to a MI, more commonly known as a heart attack [19]. In the event of a MI, a blood vessel supplying the heart becomes blocked and causes irreversible cell death if blood flow is not quickly restored. As cardiomyocytes lack the ability for regeneration, cardiac fibroblasts remodel the myocardium upon cell death into type I collagen scar tissue with limited contractility and mechanical properties, eventually leading to decreased cardiac output [17, 19]. Additionally, the site of infarction undergoes infarction expansion, where the collagen fibers in scar tissue resist the tension of the ventricular pressure and allow the myocardium to thin overtime, as shown in Figure 2 [20, 21]. This wall thinning can lead to

myocardial hypertrophy and decreased cardiac output. Patient mortality is highest when hypertrophy occurs in the left ventricle [3].

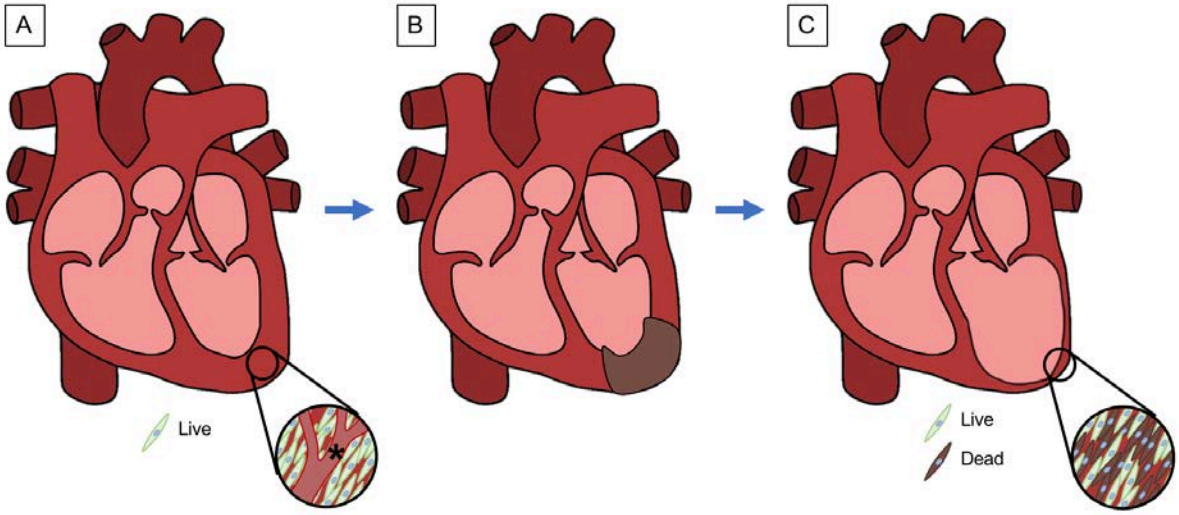

*Figure 2 After a myocardial infarction occurs in the left ventricle (denoted by a black *), (B) the cardiomyocytes die from lack of oxygen and nutrients, resulting in scar tissue formation. (C) Over time, this scar tissue yields to ventricular pressure and causes hypertrophy of the ventricle, leading to wall thinning and decreased cardiac output.*

2.2 Motivation for a Regenerative Treatment for the Left Ventricle

CVD are the leading cause of death, with 48% adults over the age of 20 having prevalence of CVD in the United States that only increases with age [1]. The total cost for treating CVD was estimated at $351.2 billion between 2014-2015, with $213.8 billion in direct costs. Currently, the only solution for treating end stage CVD is through transplantation with a donor heart. There were 3,244 heart transplants performed in the US in 2017; however, in mid-2018, there were nearly 4,000 people on the heart transplant wait list [1]. As donor hearts are in high demand, alternative procedures have been explored to restore contractile function to the myocardium to prevent end stage heart failure.

2.2.1 Clinical Treatments for Left Ventricle Replacement

Therapies for treating heart failure at earlier stages have been development in the form of surgical intervention. Additionally, the use of stem cells for renewing ventricle

myocardium is being clinically tested. Below, we examine Surgical Ventricular Restoration, current cardiac patch options, and cellular therapies currently being developed.

2.2.1.1 Surgical Ventricular Restoration

To remove scar tissue, reduce ventricular volume, and restore function shape of the left ventricle post-MI, a procedure known as Surgical Ventricular Restoration (SVR), or Dor Procedure, was developed [3, 22]. In this procedure, the scarred ventricle tissue is removed, and a cardiac patch made of decellularized matrix, pericardium, or synthetic material is placed in the myocardium, as seen in Figure 3. This procedure is often performed with a CABG, in which an autografted vessel is surgically implanted outside the heart to bypass the wounded area and return blood flow to the ventricle, and mitral valve replacement, to prevent regurgitation of blood from the left ventricle to the left atrium in the wounded system.

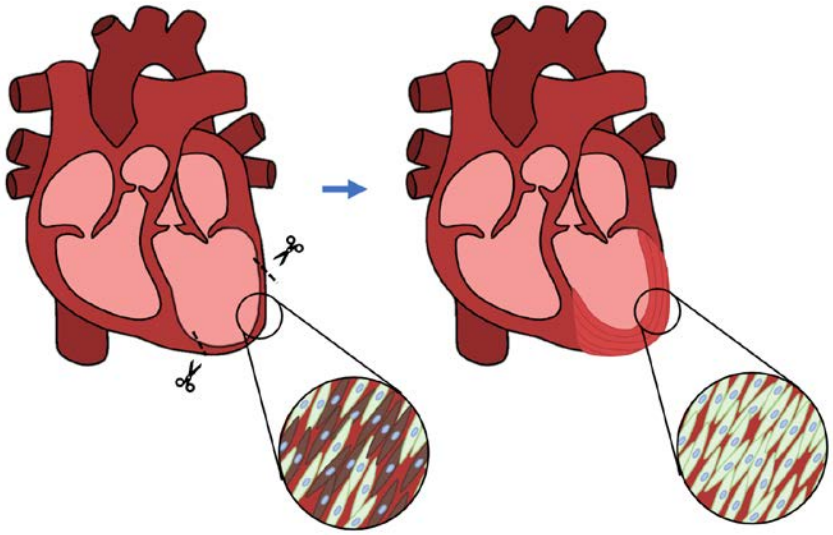

Figure 3 In SVR, diseased, thinned myocardium (left) is surgically removed and replaced with a contractile cardiac patch (right). This cardiac patch can be acellular, cellular, or designed specifically to promote ingrowth of cells.

In the 5-year post-surgical mortality rate, the mean survival for SVR patients using Dacron™ (Invista, Wichita, KS, USA) as a cardiac patch was 69%; the mean survival for CABG patients was 54%; and the mean survival for combined SVR and CABG patients was 90% [3]. These rates are, however, closely linked initial cardiac outputs and ventricle size;

ventricles initially with more advance hypertrophy and low blood ejection fractions led to a higher mortality. Additionally, an NIH-sponsored trial called STICH (Surgical Treatment for Ischemic Heart Failure) did not find any difference in patients receiving CABG and patients receiving CABG and SVR; however, there was question to the uniformity of surgeries perform in the trial [3, 23]. While SVR has not been a perfect analog to whole organ transplant, it has shown promising results for repairing patient heart function. Below, we examine several commercially available cardiac patches used for this procedure.

2.2.1.2 Cardiac Patches for SVR

Currently, several commercially available products are used in SVR: Dacron, Gore-Tex™, CorMatrix™, and multiple bovine-derived pericardium matrices [5, 24]. Dacron is a polyester fiber-based material; Gore-Tex is a Teflon-based fabric; and CorMatrix is a decellularized porcine small intestinal submucosa, most recently FDA approved in 2019 for left ventricle repair [5, 25]. All products offer different acellular material solutions for the cardiac patch solution but illicit similar immune response.

Dacron is a biologically inert woven synthetic material made of polyethylene terephthalate (PET) [3, 26]. The woven form has smaller pores compared to the knitted form, making it ideal for vascular graft engineering with its liquid-tight manufactured form. When used as a left ventricle patch in SVR, Dacron has the benefit of ease of suturing and a firm attachment [27]. The graft does, however, lead to poor cell infiltration due to its inflexible nature and the presence of a fibrous encapsulation post implantation [6].

Gore-Tex (Gore Medical, Flagstaff, AZ, USA) is a microporous sheet made of expanded polytetrafluoroethylene (ePTFE) [26]. This three-layered material is made of the elastic, microporous middle layer between two layers of polymer fibril, making it easy to

suture into place [26, 28]. Gore-Tex is also bioinert and has shown low thrombogenicity and low calcification upon implantation; however, as a bioinert material, Gore-Tex has the potential for foreign body reaction and encapsulation [4]. Additionally, Gore-Tex behaves similarly to Dacron and is rigid to contractions from native tissue, preventing the full potential for cardiac output matching that of undamaged myocardium [29].

CorMatrix (CorMatrix Cardiovascular Inc., Roswell, GA, USA), known as CorPATCH specifically for SVR, provides claims of less inflammatory response than synthetic patch materials and promotes ingrowth of native cardiomyocytes by providing natural ECM, structures, and proteins through the use of decellularized tissue [5, 25]. While there has been evidence of reabsorption of material in porcine subcutaneous studies, histology from long-term use in pediatric congenital heart surgery cases shows evidence of foreign-body giant cell reaction, fibrosis, and no tissue integration or cellular infiltration [4, 5]. While CorMatrix has shown to be a viable option for heart reconstruction, it does not support reconstitution of native myocardium.

There are also multiple patches available in the US made from bovine pericardium, including Peri-Guard™ (Baxter International, Inc, Deerfield, IL, USA), PhotoFix™ (CryLife, Kennesaw, GA, USA), SJM Biocor™ (St. Jude Medical, Saint Paul, MN, USA), and Edwards Bovine Pericardial Patch (Edwards Lifesciences, Irvine, CA, USA), as well as internationally manufactured products [24]. Additionally, the patient's own pericardium can also be used as a cardiac patch [30]. While pericardium can be functionalized to increase cell migration and adhesion to the implant, the mechanical properties of pericardium do not match that of the surrounding native tissue. As seen in synthetic materials, pericardium lacks the ability to deform with ventricular contractions [29].

These acellular materials outlined above provide passive structural support to myocardium when reshaping hypertrophic ventricle post MI; however, they are not as compliant as the native myocardium, thus contractility from any cell migration onto the scaffold would be limited [24, 29]. The lack of contracting cells offers no functional, active work to the heart and only offers passive support of ventricle shape. As many of the ECM-derived grafts are crosslinked and thus not degradable or resorbable, they will never fully integrate into the myocardium and have been shown to produce scar tissue at the implantation site, preventing full integration. There remains a significant need to develop a functional, engineered cardiac patch that easily integrates with the surrounding tissue to promote the regeneration of myocardial tissue with physiologically relevant contractility. Because of cardiomyocytes' limited ability for regeneration, the delivery of functional cardiomyocytes to the injury site would encourage contractile, function replacement myocardium that increases contractile output [15].

2.2.2 Cellular Injection Therapies

To restore the function properties of scarred myocardium, cellular based therapies have been explored to delivery cells directly to the site of injury [31, 32]. Three widely used methods are intramyocardial, intracoronary, and intravenous delivery. Intramyocardial cellular delivery can occur surgically at the myocardium, or percutaneously via transfemoral or transradial injection. Intracoronary delivery occurs by introducing cell populations through the coronary artery and into the heart [33]. It has been found that there is no safety differences between intracoronary and intramyocardial delivery; however, there is some evidence showing that intramyocardial delivery may lead to better engraftment [31, 34, 35].

Intravenous delivery is a strategy of delivering cells to the heart via intravenous injection [36]. Intravenous delivery is beneficial when delivery to the heart is not feasible, such as in the event of patients possessing prosthetic mechanical valves or pacing devices. There has been some success in increasing cardiac output through intravenous injection of human mesenchymal stem cells (hMSC) in clinical trials with no adverse health effects from the dispersion of cells to other organ systems despite minimal cell engraftment to the myocardial region [37, 38]. It is hypothesized that the main success in increased cardiac function is linked to the delivery of paracrine anti-inflammatory factors with the introduction of hMSC to the body [36-38].

An additional delivery method for cells to infarcted regions is through the use of suture delivery directly to the myocardium [39-41]. The use of a bundled fibrin microthread suture is being investigated by our collaborators through *in vivo* small animal models. By delivering hMSCs to infarcted rat ventricles, infarcted hearts showed an increase in regional mechanical function after 7 days with a decrease in infarction size compared to untreated infarctions [39]. Quantum dot labeled cells also showed migration from suture to surrounding fibrotic tissue. These results are a promising beginning to the use of a fibrin delivery system.

Two promising cell types for clinical therapies are human embryonic stem cell cardiomyocytes (hES-CM) and human induced pluripotent stem cell cardiomyocytes (hiPS-CM) [42]. hES-CM are derived from the inner cell mass of preimplantation-stage blastocysts, while hiPS-CM are derived from reprogramming adult somatic cells by forcing the expression of stem-cell transcription factors through a variety of measures [43]. hES and hiPS are both differentiated into cardiomyocytes through the expression of different set of transcription factors.

There are, however, certain disadvantages to using either stem cell type [42]. Both cell types have the potential to form teratomas after transplantation [42, 44]. Additionally, hES have an ethical dilemma surrounding them from their embryonic source and need for immunosuppressant therapy post implantation. Currently, as the state of the art of inducing hES and hiPS into cardiomyocytes progresses, both stem cell types produce limited populations of cardiomyocytes mixed in with fibroblasts that have not differentiated into fully mature cardiomyocytes; however, this rapidly evolving field may solve the problem of immature cardiomyocytes before long. Maturation to adult phenotype of hiPS-CMs have been studied through culture duration, growth hormones, substrate stiffness, and dynamic culture [45]. Additionally, immune acceptance of allogenic hiPS-CM has been studied in nonhuman primates. Transplantation of major histocompatibility complex (MHC)-matched hiPS-CM into nonhuman primates showed the potential for allogenic acceptance of hiPS-CM that partially remuscularized the region and coupled with host myocardium after 12 weeks [46]. These transplanted cells did not form tumors nor illicit an immune response, indicating the promise of a successful cellular therapy found in allogenic hiPS-CM.

Regardless of injection method or cell type, cell retention is less than 10% post implantation in human myocardium [42, 47-49]. In an injectable system, the delivery medium is often low-viscosity saline into the circulatory system. When cardiomyocytes make it to the infarcted tissue, they can have low attachment on the damaged ECM. Cardiomyocytes will die in suspension if they are unable to properly adhere. Additionally, infarcted tissue is a low oxygen environment high in inflammatory cells. Low oxygen and inflammatory cell responses can accelerate cardiomyocyte death. To ensure cell transplantation, the diseased myocardium needs to be removed from the system. This drives

the necessity of implanting a cell-seeded cardiac patch to replace damaged myocardium as well as ensure cell survival in the ventricle.

2.3 Cell-Populated Cardiac Patch

To accurately replicate human myocardium, a left ventricle cardiac patch should be 1 cm thick, generate a contractile force of 20-50 mN/mm^2, and propagate electrical impulses at 25 cm/s [32]. In addition to these specifications necessary to mimic native myocardium, there are countless other factors that must be addressed in a cell-populated cardiac patch. It must include vascularization for survival of the implanted cells and multicellular structure for proper single transduction, ECM production, and integration into the host myocardium [50].

Cell-populated cardiac patches are designed to mimic native mechanical properties, contractile output, and architecture [51, 52]. Through the delivery of cells to the injury site on a scaffold that promotes cell contractility, cell alignment is crucial to avoid arrythmias and increase synchronous contractile output [53]. By matching native cardiomyocyte alignment and conductive properties, electrical integration of implanted cells into native myocardium can occur seamlessly and prevent life threatening conditions related to delayed cell-cell conduction [54]. Here, we chose to more closely examine techniques used to increase cardiomyocyte alignment for mature tissue architecture and contractility.

2.3.1 Methods for Cardiomyocyte Alignment

Outlined below, as summarized in Table 1, are some of the current methods used to align cardiomyocytes. We have outlined three categories of commonly used techniques: tension, micropatterning, and dynamic culturing, characterized in the schematics of Figure 4.

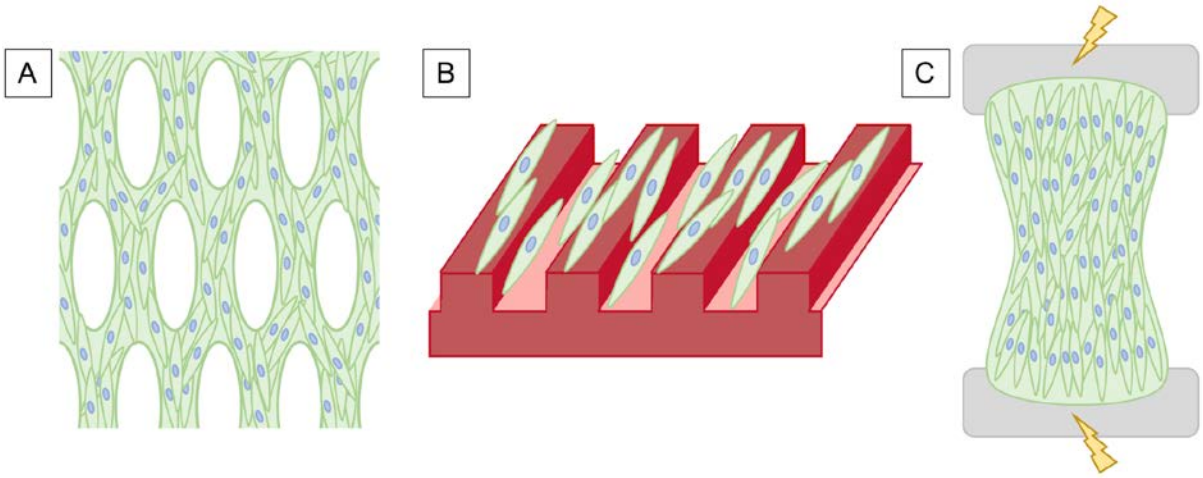

Figure 4 Three common methods of cardiomyocyte alignment are (A) tension culture, (B) micropatterning, and (C) dynamic culture, with electrical stimulation depicted here.

2.3.1.1 Tension

The use of tension culture allows for cellular alignment as cell-mediated tissue compaction occurs against molds or culturing frames. Large-scale pores have been examined by many groups as a means for creating this compaction [55-57]. As outlined by GC Engelmayr Jr, *et al*, these pores can match native myocardium mechanical response [55]. This group designed an "accordion-like honeycomb" structure with 200 µm × 200 µm square pores at 45˚ angles from each other, taking inspiration from the circumferential and longitudinal axes of the heart. Poly(glycerol sebacate) (PGS) was used to create a mechanically relevant implantable mold that was seeded with a coculture of rat heart isolations with cardiac fibroblasts that compacted after 4 days of culture. The authors found that the PGS-cardiac cell patch allowed for electrical excitation and resembled right ventricle architecture but would need to be redesigned with larger pores and a thicker patch for implantation studies. Using the same porous technology, W Bian, *et al* modified the porous design to accommodate for elliptical pores [56, 58]. Polydimethylsiloxane (PDMS) molds were created for rat neonatal ventricular myocytes (rNVM) to be cast in a fibrin-Matrigel™

hydrogel and left to culture for 2 weeks. The PDMS mold contained posts with the long axis of the elliptical at 0.6 mm and 1.2 mm. They found that the 1.2 mm pores allowed for increased cell alignment compared to the 0.6 mm pores as well as increased longitudinal conduction velocity twitch force comparable to neonatal rat myocardium. The authors found that elliptical pores allowed for controllable anisotropy.

More complex PDMS molds have been created using laser-cut acrylic molds to create pore geometry of diamonds, triangles, rectangles, and strips for an hiPS-CM seeded composite fibrin-collagen hydrogel [57]. F Munarin, *et al* saw similar compaction trends as W Bian, *et al*, but noted the porous structure made tissue handling difficult at time of implantation onto infarcted left ventricle of Sprague-Dawley rats. To overcome this, the addition of collagen into the fibrin hydrogel formulation allowed for increased mechanical properties to withstand tissue implantation, and the authors noted cells were still present in the patch as well as the infarcted surrounding tissue through histology 7 days post-surgery, indicating cells survived post-implantation and did not migrate away from engineered tissue.

2.3.1.2 Micropatterning Substrates

Surface modification can be used to direct cells migration or orientation in a process called micropatterning [59]. This can be done through coating a 2D surface in protein, growth factors, or polymers in geometries comparable to native tissue in microarrays. TC McDevitt, *et al* created PDMS with linear geometry to microcontact print laminin on thin poly(lactic-co-glycolic acid) (PLGA) films to create a biodegradable surface with aligned and differentiated rNVM [60]. Ideal geometries of 10-20 μm wide laminin lanes allowed for cells to align similarly to native rat myocardium with mature phenotypic staining. Additionally, closer lanes allowed for more synchronous beats per minute between lanes due

to cell bridging. T Pong, *et al* used the same microprinting technique to linearly pattern fibronectin on coverslips [61]. This system was designed to study the alignment and shape factor of rNVM in anisotropic system. The authors found that their anisotropic patterned geometry had increased actin filament alignment, increased cell density, and decreased cell area compared to isotropic unpatterned control. Additionally, it was determined via calcium imaging that anisotropic patterned surfaces supported higher return velocities than isotropic unpatterned controls.

In addition to the two summarized studies above, there are numerous bioactive molecules that have been used to linearly pattern cardiomyocytes on a 2D surface [62, 63]. 3D topographies have been examined through coating PDMS directly with bioactive molecules to allow for cell adherence following micro topographical cues as opposed to 2D linear cues. L Yin, *et al* used fibronectin-coated PDMS molded in a trapezoid shape with a base of 120 µm and a depth of 50 µm [64]. Through the use of calcium imaging rNVM seeded on this surface, it was found that the 3D patterned alignment had more synchronous beating compared to a 2D surface. D Motlagh, *et al* created PDMS channels coated in laminin at different depths of 2 µm and 5 µm, finding that the deeper 5 µm grooves led to increased alignment than 2 µm deep grooves and connexin-43 and N-cadherin expression comparable to neonatal rat heart [65]. The 2 µm channels did not contain enough depth to encourage cell alignment.

Additionally, the use of wrinkled polyethylene substrates has been examined to aligned hES-CM [53, 66]. These substrates were created by shrinking polystyrene films over PDMS micropatterned negative replicates for the films to pick up the micro topography. Films were then coated with Matrigel and seeded with cardiomyocytes. J Wang, *et al*

examined aligning hES-CM on this topography to study drug-induced arrythmias [66]. Usually, hES-CM are cultured in immature clusters. By culturing hES-CM on anisotopically aligned surfaces in biomimetic architecture, the authors were able to culture the cells to physiologically relevant cell organization and electrical response. AMY Shum, *et al* applied a similar technique when culturing human pluripotent stem cell cardiomyocytes (hPS-CM) [53]. These wrinkled substrates showed mature action potential and conduction velocity in two stem cell lines through inducing cellular alignment.

Groups have looked at 3D micropatterning different implantable materials as well. KMC Tsang, *et al* micropatterned a photodegradable hydrogel composed of methacrylated gelatin (GelMA) [67]. These hydrogels degrade when exposed to UV light, so the authors were able to degrade grooves in the hydrogel at specific channel geometries. Using rNVM, the scaffold support cardiomyocyte and fibroblast attachment and elongation in the direction of patterning as well as more rhythmic beating than unpatterned controls. AST Smith, *et al* utilized molded thin graphene–polyethylene glycol (PEG) films to create a contractable surface that is conducive to cell electrical coupling [68]. The graphene-PEG films were dried on a micropatterned surface to create this geometry. The micropatterned films with graphene displayed increased Z-band widths and sarcomere lengths compared to PEG alone. Furthermore, the addition of graphene allowed for an increase in cell calcium handling as well as action potential duration. In this study, micropatterning was used with a conductive material to increase cardiomyocyte electrical output.

2.3.1.3 Dynamic Environment

Culturing cardiomyocytes under a dynamic environment, such as mechanical or electrical stimulation, can lead to increased cell alignment in addition to mature phenotype

and increased electrical output. For the case of mechanical stimulation during culturing, K Chen, *et al* examined the difference in alignment of cells during 2D and 3D culture under mechanical stretch stimulation [69]. Previously, there were discrepancies in that cells cultured on a 2D surface aligned parallel to the direction of stretch while cells cultured on a 3D scaffold aligned perpendicular. By examining cardiac fibroblasts as a model for ventricular myocardium in collagen gels, the authors were able to determine that alignment, and thus cell compaction, occurred perpendicular to the direction of cyclic stretch in a 3D construct at a frequency an order of magnitude higher than that of a 2D surface. This analysis provides insight in culturing conditions necessary for highly aligned tissue as it translates from a 2D model to a 3D scaffold.

HTH Au, *et al* examined the effects of aligned topography and electric field stimulation on cell alignment and elongation [70]. Microtopography was created by microabrading coverslips and coating them with fibronectin for cell attachment. rNVM were cultured on these topographies under continuous electrical stimulation for 48 hr with the field perpendicular or parallel to the topographies. It was found that topography was a stronger determination of cellular alignment, but electrical stimulation was able to somewhat overcome topography in direction of cellular orientation.

When combining both electric and mechanical stimulation, JL Ruan, *et al* cultured hiPS-CM in collagen constructs [71]. Constructs were cultured under static stress for 2 weeks or static stress for 1 week and continuous electrical pacing for 1 week. While the

Table 1 Summary of methods for cell alignment.

Method		Examples	Summary	Reference
Tension	Mesh structure	Cell compaction around PGS frame	Cells aligned in pores while PGS allows for implantation, electrical signaling	[55]
		Fibrin-Matrigel hydrogel to analyze pore size	Increased pore size allowed for increased alignment electrical properties	[56]
		Collagen-fibrin hydrogel for better implantation handling	Implantable *in vivo* patch with cells present in patch after 7 days	[57]
Micropatterning	2D Surface	Laminin lanes on PLGA films	Architecture similar to rat myocardium	[60]
		Fibronectin lanes on coverslips	Increased contractile return velocities	[61]
	3D Model Scaffold	Fibronectin coated trapezoid PDMS channels	Synchronous beating compared to 2D surfaces	[64]
		Laminin coated 3D PDMS at 2, 5 µm depths	Increased alignment, phenotypic staining similar to rat myocardium for 5 µm grooves	[65]
		Matrigel coated polystyrene at 5 µm depth	Increased alignment, mature electrical response in hES-CM and hPS-CM	[53, 66]
	3D Implantable Scaffold	Photodegradable GelMA	Implantable hydrogel with easy to manipulate scaffold geometries	[67]
		Graphene-PEG films	Mature sarcomere structures, increased electrical coupling	[68]
Dynamic Environment	Mechanical Stretch	Biaxial stretch in 2D, 3D scaffolds	2D scaffolds align parallel to cyclic stress, 3D scaffolds align perpendicular to cyclic stress at a magnitude higher 2D frequency	[69]
	Electrical Stimulation	Microtopography, continuous electrical pacing	Topography motivates cell alignment more than electrical stimulation, electrical stimulation increased contractile output	[72]
	Mechanical Stress, Electrical Stimulation	Static stress, continuous electrical pacing	Static stress aligned cells just as well as static stress and electrical pacing, Static stress and electrical pacing increase maturity of cells	[71]

combination of the two culturing methods did not increase cellular alignment compared to static stress alone, the scaffolds cultured under stress and electrical pacing had increased contractile force, which indicts increased tissue maturity compared to static stress alone. Both tools are valuable for creating mature, contractile, and highly aligned tissue.

2.3.2 Current Limitations to the Cell-Populated Cardiac Patch

As implantable replacement myocardium is developed, there are factors limiting successful integration of engineered tissue to native tissue. Here, we will outline two complications critical to the function of the left ventricle: the foreign body response of engineered tissue and the electrical integration to native myocardium. While these two limitations can be applicable to other materials systems, they have life-threatening complications when related to the design of engineered myocardium.

2.3.2.1 Foreign Body Response

As examined in Section 2.2.1.2 Cardiac Patches for SVR, many of the current acellular patches used for left ventricle replacement illicit a foreign body response (FBR). In the later stages of the formation of granulation tissue, multinucleate giant cells form by fusing monocytes and macrophages in order to digest materials greater than 50-100 μm [73]. The presence of these multinucleate giant cells, known as foreign body giant cells (FBGCs), is indication of chronic irritation to the body. In the event that the material cannot be digested, fibroblasts begin to deposit ECM to wall off the material through the formation of a fibrous capsule, which has been shown in the presence of Dacron, Gore-Tex, and CorMatrix for left ventricle repair [4-6].

By encapsulating the implanted material, the cardiac patch will never fully integrate with the host myocardium and be limited in its functionalities [26]. While autologous tissue

is the gold standard for tissue replacement, this is not possible in the case of myocardial engineering. As donor tissue is scarce, homologous and low inflammatory biomaterials are being explored as alternative to limit immunogenic response in tissue engineering.

2.3.2.2 Electrical Integration to the Native Myocardium

Integrating engineered myocardium with native tissue faces challenges when it comes to preventing arrythmia [74]. Scar tissue formation or a fibrous capsule at the implanted-native tissue interface can cause serious physical blockage and decreases in electrical conductance and life-threatening conditions. Even without a physical barrier, implanted cells can have pacing differences leading to arrythmias [54].

To overcome issues with cell-cell coupling in implanted tissue to native tissue, the use of mechanical or electrical stimulation of cultured tissues has been used to prepare tissue for implantation. Electrically pacing hES-CM cells at a higher rate prior to implantation of rat myocardium has been shown to cause human sourced cells to couple to rat myocardium, and similar philosophies have been achieved in guinea pig and non-human primate hearts by electrically pacing hES-CMs at lower rates [7, 75, 76]. These culture strategies demonstrate the practice of conditioning cells prior to implantation to avoid arrythmias once implanted.

Additionally, maturation of hES-CMs and hiPS-CMs can be achieved from electrical and mechanical stimulation [77]. Changes in pacing frequency or cyclic loading over a culture period can induce maturation of stem cells to match values of human myocardium. Implanting mature engineered tissue can overcome the issue of mechanical integration with native adult myocardium. By implanting cardiomyocytes conditioned for mature cardiac output, dynamic culture of engineered tissues fulfills an unmet need in preventing

mismatched contractile properties at the interface of implanted engineered tissue and native myocardium.

2.4 Composite Cardiac Patch

Previously in the Pins Lab, a fibrin composite cardiac patch was designed utilizing fibrin microthreads embedded in fibrin hydrogel [78]. In this design, fibrin microthreads increased mechanical properties of the hydrogel, which was designed to match the passive stiffness of native myocardium and thus support cardiomyocytes growth. By culturing the patches under anisotropic tension, the microthreads helped drive cellular orientation and tissue-mediated compaction. This increase in cellular orientation led to increased contractile strain, contractile wave propagation, and contractile area compared to isotopically cultured cardiac patches. This patch design also supports laminating multiple patches with a tissue engineering vascular network to create a multilayered tissue with a vascular supply, mimicking the architecture of native myocardial tissue. The process of casting these anisotopically aligned patches (ANISO) and isotopically aligned controls (ISO) are depicted in Figure 5.

These studies were performed with fresh isolation rNVM. Since rNVM display immature cardiomyocyte phenotype and are not a clinically relevant cell type, we aim to advance the design of our composite cardiac patch by introducing a clinically relevant cell type of hiPS-CM. Additionally, we propose micropatterning the hydrogel portion of the composite cardiac patch for increase nuclear alignment. The use of electric stimulation on cardiomyocyte culture will also be introduced to the system to increase hiPS-CM contractile strains. By increasing contractile properties of introduced hiPS-CM, we aim to improve cell

alignment and contractility of our composite cardiac patch for an architecturally similar to native myocardium cardiac patch.

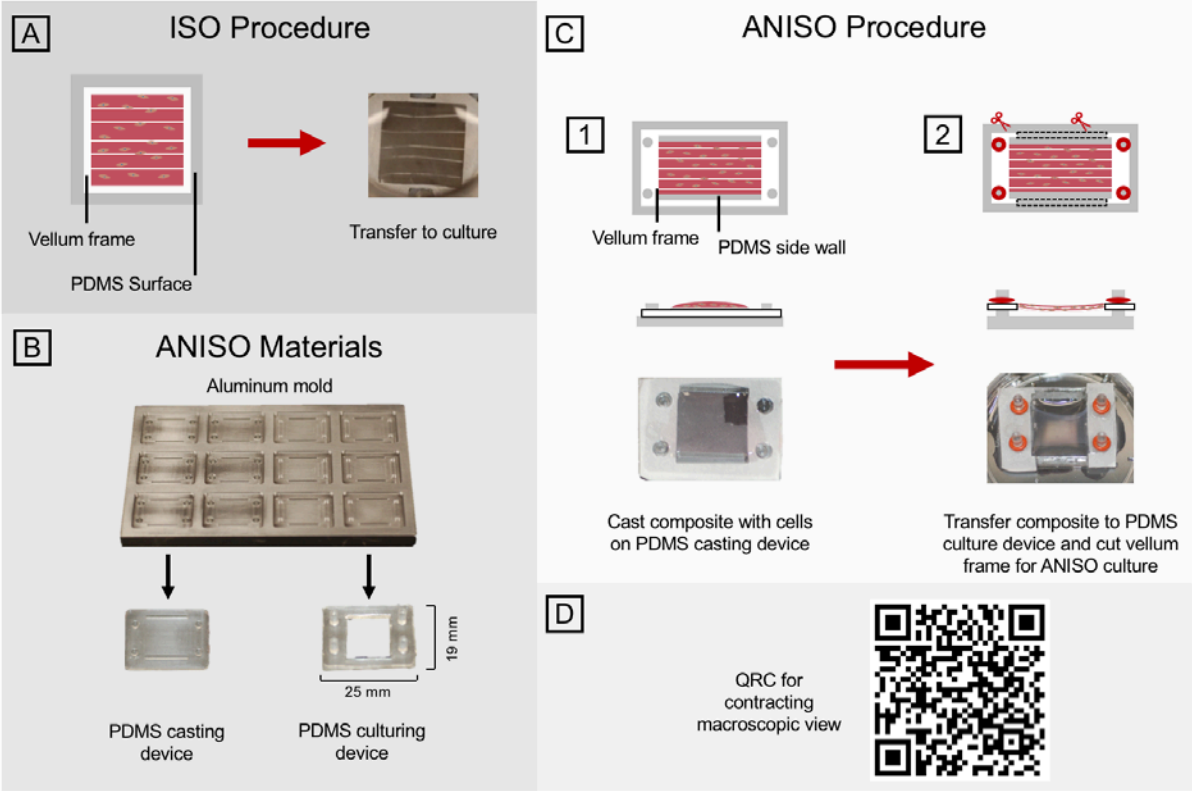

Figure 5 (A) Schematic of ISO casting procedure. Hydrogel and cell suspension are cast on Pluronics-coated PDMS surface to incorporate microthreads with constraint on all four sides. Once polymerized, samples are then transferred to culture. (B) PDMS is used with an aluminum mold to create casting and culturing devices that couple with vellum frames. (C) Schematic cartoons of top and side views as well as images of scaffolds show (C1) the Pluronics-coated PDMS casting device which constrains the hydrogel anchoring it to the two opposing sides of the vellum frames. Cell-seeded fibrin hydrogels are cast into microthread-loaded frames to create the engineered composite. (C2) For ANISO culture, samples are transferred to the PDMS culturing device, secured with o-rings and the sides of the frames are removed for anisotropic tension culture. (D) QRC code linked to macroscopic view of contracting composite patch.

Source: Chrobak MO, English EJ,…,Pins GD. "Anisotropic Tension Increases Cardiomyocyte Alignment and Contractile Strain in Composite Fibrin Scaffolds." 2019. In Submission.

2.5 Project Materials

The following materials were selected for use in the micropatterned cardiac patch. Fibrin hydrogel's role in wound healing and angiogenesis makes it a viable material for cell delivery to the injury site, and hiPS-CM have the future potential to be autologously sourced, preventing immunological response. Electrical stimulation has been shown to increase

contractile properties and maturation in hiPS-CM culture as well as integration with engineered ventricle to native myocardium. By using these materials, we can create a contractile cardiac patch with physiologically relevant cell alignment.

2.5.1 Micropatterned Fibrin Hydrogels

In regenerative medicine solutions, a provisional ECM scaffold is used to transplant cells to the wound site [79]. While there are a variety of synthetic materials used as a scaffold for engineered tissue, such as polyglycolic acids (PGA) or polylactic acid (PLA), and natural materials, such as collagen or chitosan, this cardiac patch was made with fibrin hydrogel [10, 80]. Fibrin occurs through the enzymatic conversion of fibrinogen by thrombin and is essential to blood clotting in early stages of wound healing. Fibrin's role in wound healing thus makes it noninflammatory and proregenerative. Because it is made of blood products, it also has the potential to be patient specific. It has previously been used as a cardiac tissue scaffold because of its tunable mechanical properties, native angiogenic properties, and biocompatibility [80-82]. Since fibrin can be used as an injectable hydrogel in an ischemic model and conforms to native geometries during polymerization, it is an ideal scaffold to be micropatterned for cardiomyocytes delivery.

2.5.2 hiPS-CM from Cellular Dynamics International

This project used hiPS-CM because of their ability to differentiate indefinitely and the potential to be tailored to patient specific applications to prevent immunological response [42]. Additionally, allogenic hiPS-CM have been shown to couple to nonhuman primate hearts, opening the window of possibility for large scale batch production of hiPS-CM for clinical use [46]. For this research, Fujifilm's Cellular Dynamics International (CDI; Madison, WI, USA) were chosen as a source of hiPS-CM [83]. CDI's iCell Cardiomyocyte^2

are a human sourced hiPS-CM that provide rapid recovery of electrical activity in the form of spontaneous beating from cryopreservation. Additionally, the custom medium limits the small population of non-cardiomyocytes from proliferating as well as supporting extended culture times. iCell Cardiomyocyte^2 are a viable option for future expansion and manufacturing because of their good laboratory practices (GLP) batch availability in industrial-scale quantities.

2.5.3 Continuous Electrical Stimulation from IonOptix C-Pace

IonOptix's C-Pace Cell Culture Stimulator (Westwood, MA, USA) was used to continuously electrically simulated our cardiac patches for increased contractile properties [84]. The C-Pace System allows for simultaneous stimulation of six samples in a standard 6-well dish with solid, non-toxic carbon electrodes. The C-Pace system has the capabilities to input stimulation frequency, pulse duration, voltage, and stimulation holds. With its customizable protocol, the C-Pace system can be integrated into a cardiomyocyte culture without switching equipment to optimize stimulation protocols.

2.6 Summary

In the event of a MI, ischemic conditions induce cell death and lead to the formation of noncontractile scar tissue. The scarred ventricle undergoes remodeling, causing a thinning of the myocardium, enlarging the ventricle chamber, and reducing functional output. Because of cardiomyocytes limited ability to regenerate, the only long-term therapy available for heart failure is a heart transplant; however, there is limited availability of healthy donor tissue. Intermediate therapies involve replacing the left ventricle with a cardiac patch through SVR, but the current materials available are acellular synthetics or decellularized bovine- or

porcine-based materials. These materials do not fully integrate into the myocardium and lead to fibrous encapsulation, thus requiring an eventual whole-organ transplant.

We propose the use of a cellular-based cardiac patch to replace noncontractile scar tissue with contractile engineered heart tissue. hiPS-CM will be micropatterned to induce alignment and cultured under continuous electrical stimulation to increased contractile output. The micropatterned scaffold will be produced with fibrin hydrogel because of its role as a natural wound healing provisional matrix and, like hiPS-CM, have the potential to be made from autologous sources. Conditioning hiPS-CM on an implantable, contractile surface is an initial step to producing a physiologically relevant replacement for ventricular myocardium.

Chapter 3 Hypothesis and Specific Aims

The overall goal of this project is to advance our composite fibrin microthread-hydrogel cardiac patch by increasing the nuclear alignment. We propose the use of micropatterning the hydrogel portion of the patch for increased cardiomyocyte alignment. Additionally, we will investigate the use of electrical stimulation in cardiomyocyte culture in the direction of nuclear alignment. When used in combination with topographical cues, electrical stimulation has the potential to increase cardiomyocyte contractile properties. For this system, hiPS-CM will be used as a clinically relevant cell type to focus efforts of increasing alignment, maturation, and contractility. This thesis will focus on examining the effects of micropatterning and electrical stimulation without the composite fraction in order to independently assess the effects they have on the system. Therefore, **we hypothesize that micropatterning fibrin hydrogels for the use of a cardiac patch will increase cardiomyocyte alignment that, along with culturing under electrical stimulation, will promote increased contractile strain compared to unpatterned hydrogel.** This thesis is divided into three specific aims:

3.1 Specific Aim 1: Develop fibrin scaffolds with aligned surfaces to increase nuclear orientation.

The goal of Aim 1 is to increase cellular alignment on fibrin hydrogels through micropatterning. A surface for casting fibrin hydrogels will be designed and fabricated with aligned topographical features for nuclear alignment. Using photolithography, micropatterned substrate and a PDMS negative replicate will be created to form a casting surface for fibrin hydrogels which will micropattern during gel polymerization. We will analyze the fidelity of micropatterns on the surface of hydrogels with respect to the PDMS

negative replicates, and an initial confirmation of nuclear alignment will be done using C2C12 murine myoblasts. Multiple topographies will be examined to determine the geometry that maximizes nuclear alignment.

3.2 Specific Aim 2: Determine topographic features that maximize hiPS-CM cellular morphology.

In Aim 2, we hypothesize culturing hiPS-CM on micropatterned hydrogels will result in increased cellular alignment compared to unpatterned controls, resulting in a more mature cardiomyocyte phenotype. The effects of micropatterning on hiPS-CM phenotype will be examined in this aim. We will characterize the nuclear alignment of hiPS-CMs on micropatterned hydrogels, as well as expression of sarcomeric α-actinin and connexin-43 through immunohistochemistry. Sarcomeric α-actinin morphology and the location connexin-43 in the cell indicate functional, mature hiPS-CM, so 7 days of culture will be compared to 14 days for any visual differences. Additionally, we will analyze the distribution of focal adhesion complexes for hiPS-CMs on patterned substrates to characterize cell directionality. Vinculin will be studied as the focal adhesion of interest for its interactions with the proteins necessary to stabilize connexin-43 expressing gap junctions. By analyzing cellular function with regards to micropatterned scaffolds, the maturity of cardiomyocytes can be characterized for this scaffold system. We anticipate an increase in cell alignment will

display more mature cardiomyocyte phenotype compared to unpatterned controls as well as an increase in directionality of vinculin staining.

3.3 Specific Aim 3: Characterize the contractile strain response of hiPS-CM seeded micropatterns to electrical stimulation.

In this final aim, we hypothesize culturing hiPS-CM seeded micropatterned fibrin hydrogels with continuous electrical stimulation for 7 days will yield a higher contractile strain of hiPS-CM compared to static cultured controls. Contractile strain will be used to measure functional differences in electrically paced scaffolds compared to a static culture. Strain will be measured using a custom pixel tracking algorithm on high-speed contraction videos. We anticipate an increase in contractile strain compared to unpatterned controls as well as an increase in contractile strain compared to static cultured constructs.

Chapter 4 Materials and Methods

The following section outlines the methods used to fabricate and analyze micropatterned hydrogels, analyze hiPS-CM phenotype, and analyze hiPS-CM contractile function.

4.1 Production of Micropatterned Silicon Wafer

To create micropatterned surfaces, photolithography was used to create a master silicon wafer [85]. DraftSight software (Dassault Systemes, Waltham, MA, USA) was used to create a high-resolution transparency mask of microchannels with plateau and width spacing of 10, 15, 25, 50, and 100 µm and was printed at CAD/Art Services, Inc. (Bandon, OR, USA) at 25,000 dpi, as depicted in Appendix A. An SU-8 2035 photoresist coated silicon wafer was created using standard photolithographic techniques with a depth of 20 µm. Briefly, a silicon wafer was baked at 200˚C for 5 min on a hotplate to dry the wafer. The wafer was then transferred to a wafer spin coater (model WS-650-23B, Laurell Technologies Corporation, North Wales, PA, USA) where ~4 mL of SU-8 2035 photoresist (MicroChem, Westborough, MA, USA) was added to the center of the wafer. The spin coater was then run to spread the photoresist at 100 RPM/sec ramping up to 500 RPM/sec and then coat the wafer to 20 µm deep photoresist at speeds ramping up to 3000 RPM/sec. The wafer was then soft baked for 2 min at 65˚C and 5 min at 95˚C. The coated wafer was then UV exposed to the photo mask using a UV-KUB UV exposure unit (Kloe, Montpellier, France) at 200 mJ/cm^2. The wafer was then post baked for 1 min at 65˚C and 2 min at 95˚C. It was developed by agitating and rinsing for 2 min in SU-8 developer (MicroChem), rinsed with isopropanol, and hard baked to cure for 2 min at 200˚C. The wafer was then coated in liquid fluorine 24 hr prior to initial use to encourage release of polydimethylsiloxane (PDMS; Sylgard 184, Dow

Corning, Midland, MI, USA) negative replicates of the wafer. PDMS negative replicates from the master silicon wafer were created by mixing PDMS at a ratio of 1:10 and curing overnight at 60˚C to create a castable surface for fibrin hydrogels. The abbreviated creation of cell-seeded scaffolds is outlined in Figure 6A.

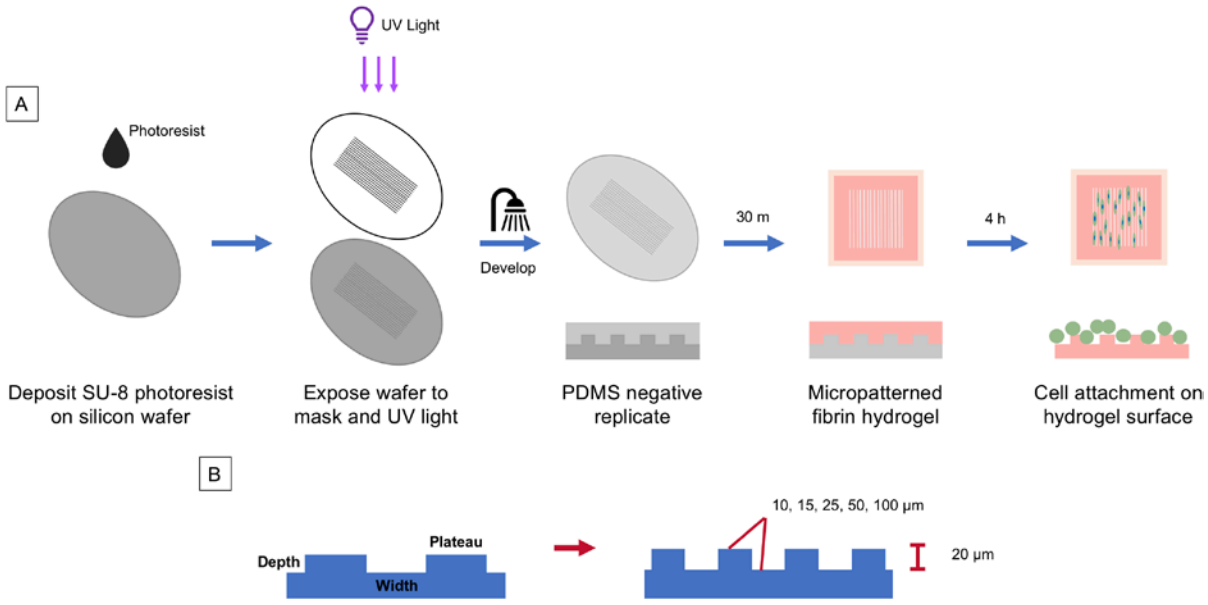

Figure 6 (A) SU-8 photoresist is deposited on the silicon wafer, which is then exposed to UV light and the photomask. The UV light crosslinks the photoresist where it is able to pass through the clear parts of the mask, and the parts that are prevented from crosslinking are rinsed off in developing. Once the silicon wafer is ready for use, a PDMS negative replicate is taken of the wafer by curing the PDMS overnight at 60˚C. The PDMS is then coated in 1% Pluronics, and a 10 mg/mL fibrin hydrogel is cast on the surface. After 30 min of polymerization, the micropatterned hydrogel is seeded with 200,000 hiPS-CMs for 4-6 hr before it is transferred to culture. (B) Hydrogels were designed with channel geometry with the plateau and width having the same dimensions of 10, 15, 25, 50, or 100 µm. All micropatterned hydrogels were designed to have a depth of 20 µm.

4.2 Fabrication of Micropatterned Hydrogel

PDMS negative replicates were autoclaved and coated in sterile 1% Pluronics-F127 in deionized water (Sigma, St. Louis, MO, USA) for 1 hr. Vellum frames with an inner dimension of 1.2×1.2 cm^2 were ethylene oxide sterilized and placed on top of the PDMS negative replicate. In a sterile environment, a sterile hydrogel solution of 90.7% 11 mg/mL bovine plasma fibrinogen (MP Biomedicals, Santa Ana, CA, USA), 4.0% 1.6 U/mL bovine plasma thrombin (Sigma), and 5.3% Dulbecco's Modified Eagle Medium (DMEM, Thermo Fisher Scientific, Waltham, MA, USA) was mixed on ice, and 150 µL of solution was spread

in an even layer onto the vellum frame. Hydrogels were allowed to polymerize for 30 min at room temperature in the biological safety cabinet. Unpatterned hydrogels (0 µm) were cast on a separate, flat piece of PDMS. In the event of cell seeding, cells were seeded onto the micropatterned side of the hydrogel immediately after polymerization.

4.3 Characterization of Fidelity of Micropatterned Fibrin Hydrogels and PDMS Negative Replicates

Hydrogels with micropattern channel geometry of 10, 15, 25, 50, and 100 µm were characterized. To determine the fidelity of the PDMS negative replicates, three separate PDMS negative replicates were sectioned with a razor blade and brightfield imaged at 10× or 20× using a Nikon Eclipse E600 microscope (Melville, NY, USA). Three length measurements per image for plateau, width, and depth were taken in ImageJ (NIH) (N = 3).

To determine the fidelity of the micropatterned fibrin hydrogels, hydrogels were cast, rinsed three times in phosphate buffered saline (PBS, EMD Chemicals, San Diego, CA, USA), and stored in PBS at 4˚C overnight. Rhodamine dye (Sigma) was prepared at a concentration of 0.1 mg/mL in PBS. Hydrogels were dip-coated in dye, dabbed to remove excess dye on a Kimwipe (Kimberly-Clark, Irving, TX, USA), and imaged at 20× and 40× using a TCS SP5 Point Scanning Confocal microscope (Leica, Buffalo Grove, IL). A 3D projection was created in ImageJ using the orthogonal view, and three length measurements per image for plateau, width, and depth were taken in ImageJ ($N \geq 7$) as outlined in Figure 7. A dimensional ratio of hydrogel to PDMS negative replicate was calculated to determine trends in fidelity.

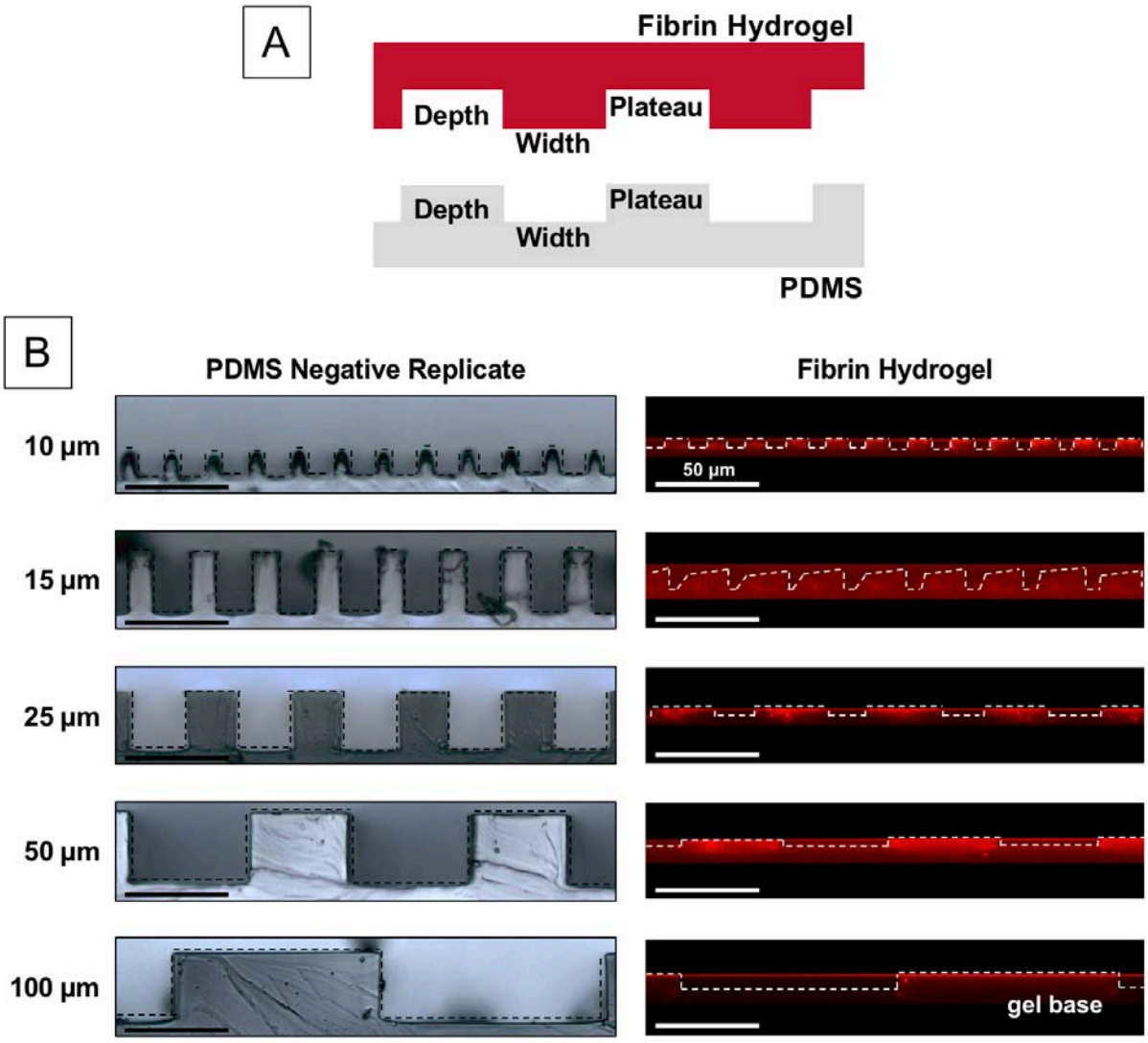

Figure 7 (A) Plateau, width, and depth were defined for PDMS negative replicates and fibrin hydrogels. (B) Measurements of PDMS negative replicates and fibrin hydrogels were taken in ImageJ as noted by the dotted outlines.

4.4 Analysis of C2C12 Nuclear Alignment

Hydrogels with micropattern channel geometries of 0, 10, 15, 25, 50, and 100 µm were characterized. Murine skeletal myoblasts (C2C12, American Type Culture Collection (ATTC), Manassas, VA, USA) were used as a model cell type to determine the initial nuclear orientation of cells seeded onto micropatterned fibrin hydrogels because of skeletal muscle's affinity for alignment to create functional myotubes. C2C12s were cultured with medium

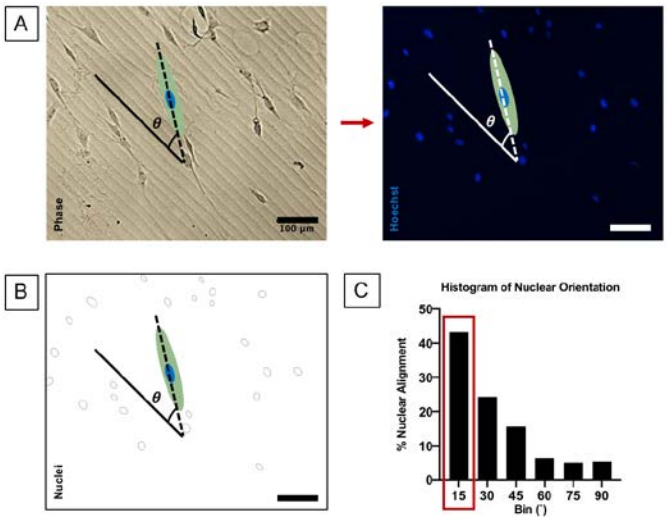

Figure 8 (A) The angle of the nucleus is measured against the direction of the pattern surface for the nuclei stain the DAPI channel. (B)A binary image of the DAPI channel is analyzed in ImageJ to find the nuclear angle. (C) A histogram of percent nuclei in each binning group is created. Each group represents the angle of the nuclei from the direction of the micropatterns. 15˚ denotes alignment.

containing a 1:1 ratio of high glucose DMEM and Hams Nutrient Mixture F12 (Thermo Fisher Scientific), 10% fetal bovine serum (Thermo Fisher Scientific), 1% penicillin-streptomycin (Thermo Fisher Scientific), 1% amphotericin B (Sigma), and 0.04% aprotinin (Sigma). Briefly, cloning cylinders with an inner diameter of 8 mm (Pyrex, Corning, Inc., Corning, NY, USA) were placed on the hydrogels to seed 25,000 cells in 100 µL. Cells were seeded at a low cell density to determine effects of the substrate on cell alignment independent of cell-cell signaling. Cells were left to adhere for 2 hr at 37˚C, 5% CO_2 before removing the cloning cylinders, rinsing samples once with medium, and cultured in new wells overnight. Cells were cultured for 24 hrs to encourage full attachment and elongation but to limit the effect of proliferation. Samples were then fixed with 4% paraformaldehyde, permeabilized with 0.1% Triton, stained with 1:40 Alexa Fluor 488 Phalloidin (Life Technologies, Waltham, MA), and counterstained with 1:6000 Hoechst (Thermo Fisher Scientific) at room temperature. Samples were then imaged at 10× using a Nikon Eclipse E600 microscope. For each sample, two distinct regions were imaged ($N \geq 6$).

To determine the alignment of cells on micropatterned hydrogels, a binary image of the DAPI channel was analyzed in ImageJ. The particle analysis function was used to obtain

orientation of the long axis of the nucleus with respect to the microchannel direction, as seen in Figure 8A-B. The angles were then corrected to fall within 0˚ and 90˚, with 0˚ indicating perfect parallel alignment and 90˚ indicating perfect perpendicular alignment. These values were binned in 15˚ increments and plotted as a histogram to present the distribution of nuclear orientations observed for each group, as seen in Figure 8C. The binning group 15˚ closest to the direct of the micropattern, as well as the mean angle for each surface, were then analyzed.

4.5 hiPS-CM Thawing and Seeding

Culturing of hiPS-CMs was adapted and modified from manufacture specifications [83]. Briefly, cells were thawed for less than 4 min in a 37˚C water bath and transferred to the biological safety cabinet. Cells were added to a 50-mL conical tube using a 1 mL pipettor, and the empty cryovial was rinsed with 1 mL of room temperature Plating Medium (FUJIFILM Cellular Dynamics, Inc.). This rinse was added to the conical tube dropwise over 90 sec with a 1 mL pipettor. An additional 3.5 mL Plating Medium was added to the conical tube using a 5-mL serological pipette dropwise over 60 seconds. Cells were then centrifuged for 5 min at 1000 rpm in an IEC Centra CL 2 centrifuge (Thermo Fisher Scientific) and resuspended in Plating Medium at a concentration of 2×10^6 to 2.5×10^6 cells/mL. Cells were swirled to mix, and 100 µL of cell suspension was seeded on hydrogels using cloning cylinders or on 1 × 1 cm 0.67% gelatin coated coverslips for 4-6 hr at 37˚C, 7% CO_2. Samples were then rinsed once with 37˚C Maintenance Medium (FUJIFILM Cellular Dynamics, Inc.) and 0.4% aprotinin before being cultured in the same medium at 37˚C, 7% CO_2. Medium was changed every other day.

4.6 Analysis of hiPS-CM Nuclear Alignment

A measure of nuclear alignment was performed using hiPS-CM to validate the alignment of hiPS-CM on micropatterned hydrogels. Hydrogels seeded with 2×10^5 to 2.5×10^5 hiPS-CM were cultured for 7 days to achieve full attachment and maturation according to manufacture specifications (Appendix B) ($N \geq 5$). Analysis was performed in ImageJ as outlined in Section 4.4 Analysis of C2C12 Nuclear Alignment.

4.7 Cardiomyocyte Phenotypic Analysis

To confirm cardiomyocyte phenotype, hiPS-CM-seeded coverslips and 0, 10, and 100 µm hydrogels were immunostained to assess the maturity of sarcomeric structure and connexin-43 expression. Samples cultured for 7 days and 14 days with spontaneous beating occurring within the first 18 hr were fixed with 4% paraformaldehyde, permeabilized with 0.1% Triton, and blocked with 5% goat serum (Invitrogen) in PBS. Samples were incubated for 60 min with mouse monoclonal to sarcomeric α-actinin primary antibody (Abcam, Cambridge, MA), and rabbit polyclonal to connexin 43 (Abcam) in blocking solution at a dilution of 1:100. Samples were then incubated with secondary antibodies (goat anti-mouse Alexa Fluor 546, Life Technologies and goat anti-rabbit Alexa Fluor 488, Life Technologies) at room temperature for 30 min at a dilution of 1:200 before being

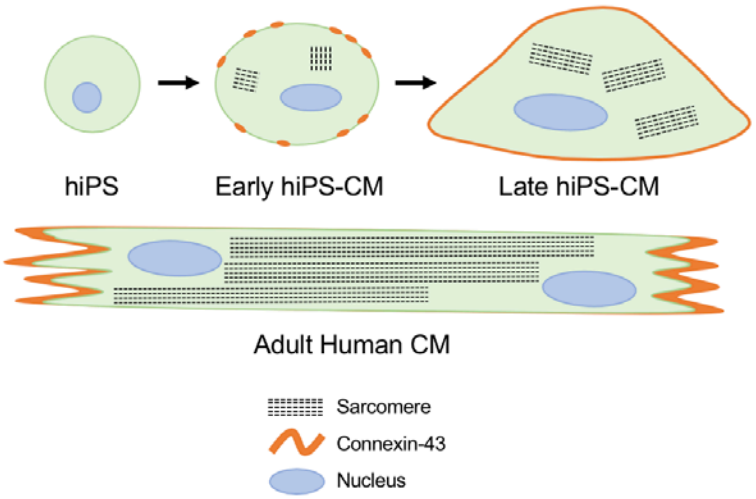

Figure 9 Sarcomere and connexin-43 phenotype of maturing hiPS-CM compared to adult human cardiomyocytes.

Adapted from Robertson C, et al. Stem Cells. 2013.

counterstained with 1:6000 Hoechst. Samples were imaged at 63× on a TCS SP5 Point Scanning Confocal microscope. The phenotypic maturity of cells was assessed for changes at days 7 and 14, as summarized in Figure 9.

4.8 Vinculin Analysis of Cardiomyocytes on Micropatterned Hydrogels

Vinculin staining was visualized on hiPS-CM seeded coverslips and 0, 10, and 100 µm hydrogels. Samples were fixed at 48 hr post-seeding with spontaneous beating occurring within the first 18 hr. Samples were fixed with 4% paraformaldehyde, permeabilized with 0.5% Triton, and blocked with 10% goat serum in PBS. Samples were incubated overnight with rabbit monoclonal to vinculin primary antibody (Abcam) in blocking solution at a dilution of 1:100 then following with 30 min of secondary antibody (goat anti-rabbit Alexa Fluor 594, Life Technologies) at room temperature at a dilution of 1:40. Samples were then stained with 1:40 Alexa Fluor 488 Phalloidin and counterstained with 1:6000 Hoechst at room temperature. Samples were imaged at 63× with a 2× zoom on a TCS SP5 Point Scanning Confocal microscope.

4.9 Continuous Electrical Stimulation of Cardiomyocytes on Micropatterned Hydrogels

The effects of continuous electrical stimulation of hiPS-CM seeded micropatterned hydrogels were analyzed for coverslips and 0, 10, and 100 µm hydrogels. After scaffolds were seeded for 24 hr with spontaneous beating starting within 18 hr, samples were moved to custom ethylene oxide sterilized 6-well dishes designed to anchor the micropatterns parallel to the electric field stimulation. A sterile 6-well C-Pace electrode was placed over the stimulated samples, and samples were cultured at 1 Hz, 5 V/cm, and 4 ms waveforms, similar to that of human myocardium, continuously for 7 days with an anchored, unstimulated plate as control [7]. C-Pace stimulation was visually confirmed using a bright field microscope.

Electrodes were changed every other day with medium changes to prevent mineralization of the carbon electrodes. High-density mapping (HDM) was performed on the final day for all samples.

The 6-well C-Pace electrodes were cleaned by soaking the electrodes in deionized water with a stir bar for at least 24 hr, changing the water at least three times. Electrodes were then scrubbed with a soft bristled brush, rinsed with deionized water, and allowed to fully dry. Electrodes were then submerged in 70% ethanol for at least 2 hrs for sterilization. The electrodes were then rinsed twice with sterile DI water for 5 min and allowed to dry completely in the biological safety cabinet. Prior to introducing the electrodes to samples, they were UV sterilized for at least 30 min.

4.10 High-Density Mapping (HDM) Analysis of Cardiomyocyte Contractile Strain

High-density mapping (HDM) was performed to measure the contractile strain of micropatterned hydrogels cultured under continuous electrical stimulation and static conditions. Samples were removed from electrical pacing 30 min prior to imaging. Videos of minimum 5 contractions (~500 frames) were collected at a frame rate of 60 fps (frames per second) at 10× phase using a Leica DMIL inverted microscope and a HiSpec4 high-speed camera (Fastec, Inc., Marlborough, MA, USA). A custom MATLAB (MathWorks, Natick, MA, USA) algorithm was used to perform HDM as previously described [86-88]. Briefly, a region of interest (ROI) was chosen of the entire image size (approximately 1200 × 120 µm), and this ROI was divided into 16 × 16 pixel subwindows. The displacement of each subwindow was tracked in

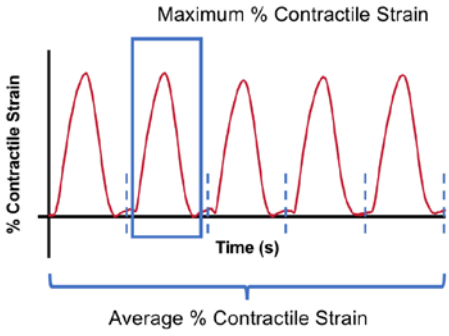

Figure 10 Average contractile strain as defined as the average strain over five contractions, and maximum contractile strain as defined as the maximum contraction in a video.

sequential frames at pixel shifts half the window size (8 pixels) in the x and y directions. The percent average contractile strain and percent maximum contractile strain over the entire region could then be calculated for each video ($N \geq 6$). Percent average contractile strain and percent maximum contractile strain are defined in Figure 10. Percent contractile strain is calculated by HDM by the changes in length of pixel shifts over the original length.

4.11 Statistics

Values are reported as mean±standard error of the mean (SEM). Normality was determined using Shapiro-Wilk Test. In the event of comparison between only micropatterned hydrogels, a one-way analysis of variance (ANOVA) with $p < 0.05$ indicating significance was used with Tukey's multiple comparison test. If data was not normally distributed, a Kruskal-Wallis Test with $p < 0.05$ was used with Dunn's multiple comparison test. In the event of comparison between micropatterned hydrogels and culture conditions, a two-way ANOVA with $p < 0.05$ indicating significance was used with Sidak's multiple comparison test. Outliers were identified using the interquartile range (IQR) in Microsoft Excel (Redmond, WA, USA) and removed if they were greater than the maximum value or less than the minimum value. All plots and statistics were generated using GraphPad Prism (San Diego, CA, USA).

Chapter 5 Results

5.1 Specific Aim 1: Develop fibrin scaffolds with aligned surfaces to increase nuclear orientation.

The goal of this first study is to develop micropatterned fibrin hydrogels to increase cardiomyocyte alignment. The design process will be summarized, and then the morphology of the hydrogels will be examined compared to their design. Alignment of myoblast model cells C2C12 seeded on micropatterned hydrogels are analyzed.

5.1.1 PDMS Photolithography Allows for the Fabrication of Micropatterned Hydrogels

The entire process of photolithography from mask design to micropatterned hydrogel formation is outlined in Figure 6. On the photolithography mask in Appendix A, each pattern was designed to alternate black and clear bands of the same widths so that the upper plateau would match the width at the bottom of the channel. This was repeated for the 10, 15, 25, 50, and 100 µm channel geometries. Because of the resolution of the photolithography mask can be used to dictate the printed geometries, we were able to print a mask allowing for specific geometries as small as 10 µm [89]. Each pattern was copied five times so that one PDMS negative replicate would have the ability to create multiple hydrogels of the same condition.

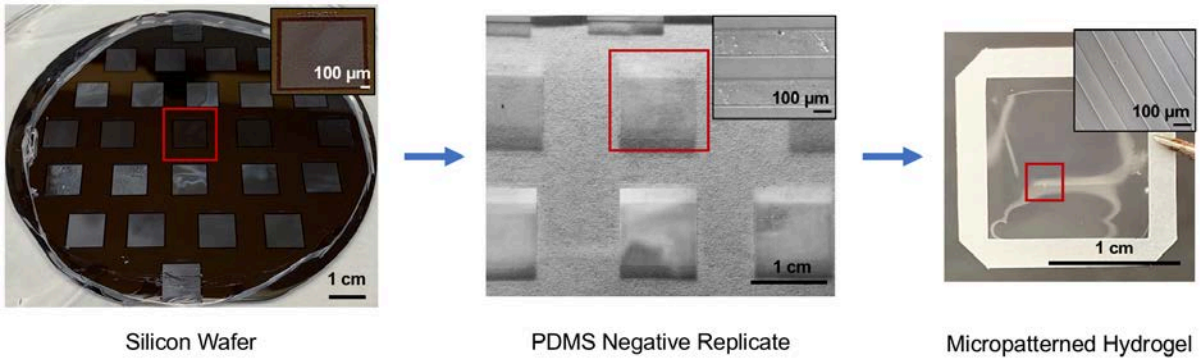

Figure 11 The micropatterned silicon wafer (A) cast a PDMS negative replicate (B) which could be used to micropattern a fibrin hydrogel (C). Inserts show 100 µm design.

The micropatterned silicon wafer was created by exposing the photolithography mask to UV light and cross-linking the SU-8 photoresist on the wafer, as shown in Figure 11A. Patterns that appeared damaged or partially formed once the PDMS negative replicate was taken of the silicon wafer were discarded and not used to cast micropatterned hydrogels. Micropatterned hydrogels were cast on the PDMS negative replicates and conformed to the channel geometry (Figure 11B-C).

5.1.2 Micropatterned Hydrogels Retain Channel Geometry and a Reliable Replication of Micropattern Depth

Confocal z-stacks of micropatterned hydrogels coated rhodamine dye were processed in ImageJ to give the orthogonal view of the micropatterned hydrogel, and the PDMS negative replicate was sectioned with a blade and imaged in bright field, as seen in Figure 12. Rhodamine dye and confocal imaging was used to measure hydrogel dimension as opposed to histology because of the distortion and shrinkage of hydrogels that occurs during histological processing (Appendix C). Distinct channel geometry of the micropatterned hydrogels can be seen in the orthogonal and aerial views of the hydrogel. The geometry of the orthogonal micropatterned hydrogels is similar to the of the PDMS negative replicates.

Using the PDMS sections and micropatterned hydrogel orthogonal view, the fidelity of the hydrogels was measured and compared (Figure 13). The dimension of the depth, width, and plateau, as defined in Figure 6B, were measured in ImageJ and compared to one another. The plateau and width dimensions of the PDMS negative replicates exhibited a variety of geometries available to cast hydrogels on, ranging from 12.1×5.5 μm for the

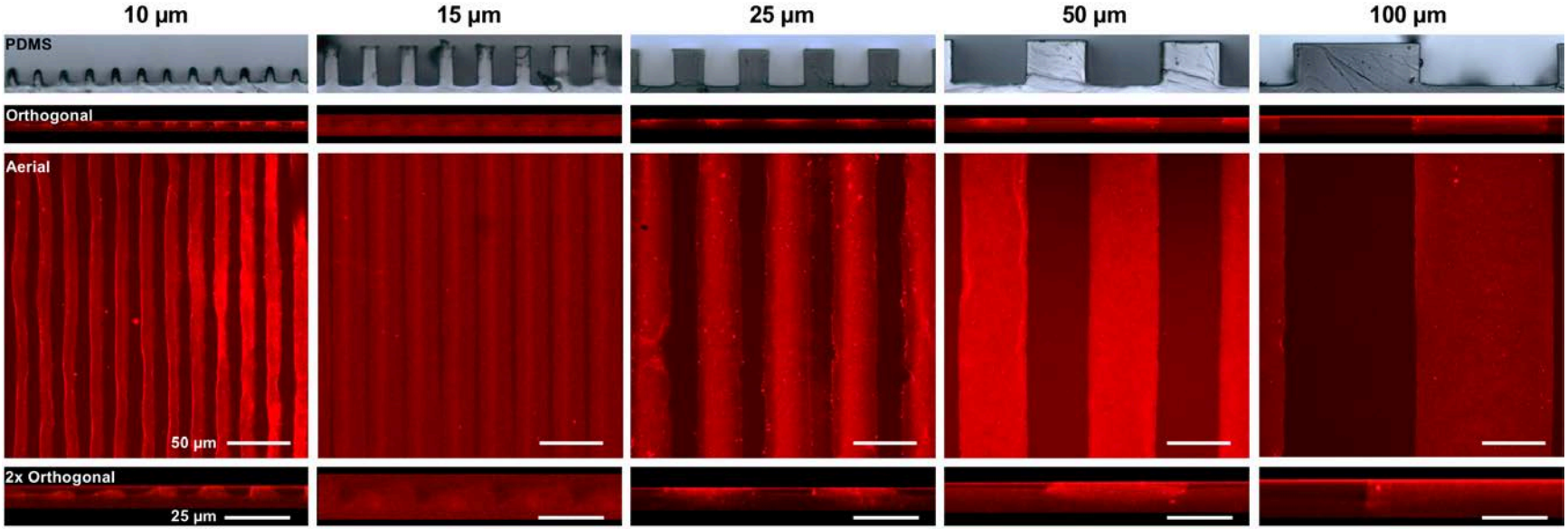

Figure 12 Sectioned PDMS negative replicates were imaged in bright field (PDMS), while confocal z-stacks were taken of rhodamine dyed hydrogels. These z-stacks were processed to the orthogonal view in ImageJ (Orthogonal), while a representative slice of the z-stack is shown for the aerial view (Aerial). A 2× magnification of the orthogonal view is shown in the bottom row (2× Orthogonal).

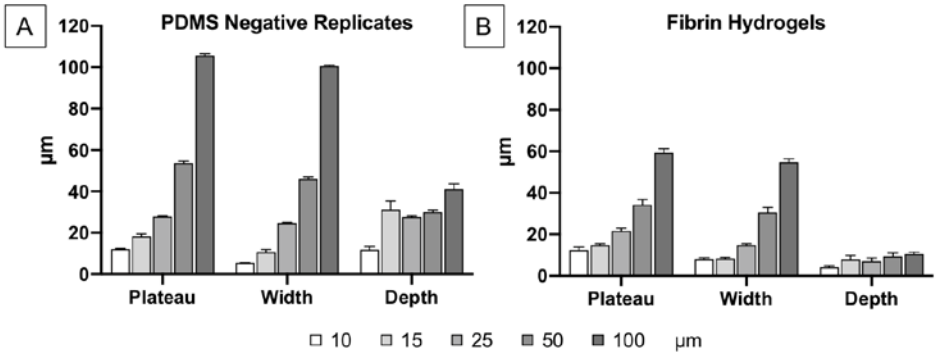

Figure 13 The geometry of the PDMS negative replicates (A) and micropatterned hydrogels (B) were measured to determine the fidelity of the patterned fibrin hydrogel. Mean±SEM, N = 3 for the PDMS negative replicates, N ≥ 7 for the fibrin hydrogels.

10 µm hydrogels to 105.7 × 100.5 µm for the 100 µm hydrogels. The depths ranged from 11.8 µm to 41.1 µm, increasing with predicted channel geometry.

Figure 12 depicted fibrin hydrogels conformed to similar geometries as the PDMS negative replicates. To better understand the fidelity of the PDMS negative replicates and the micropatterned hydrogel, the dimensions of the topographies were measured in Figure 13. This fidelity was then analyzed by examining the fibrin hydrogel to PDMS negative replicate ratio in Table 2. The hydrogel's plateau and width measurements were less than the PDMS negative replicate's measurements for all hydrogels except the 10 µm hydrogels. The hydrogel depth was always 0.3 that of the PDMS negative replicate.

Table 2 Fibrin Hydrogel: PDMS Negative Replicate Ratio

Ratio of Fibrin Hydrogel: PDMS Negative Replicate			
Dimensions	**Plateau**	**Width**	**Depth**
10 µm	1.0	1.4	0.3
15 µm	0.8	0.8	0.3
25 µm	0.8	0.6	0.3
50 µm	0.6	0.7	0.3
100 µm	0.6	0.5	0.3

5.1.3 C2C12 Nuclei Have Increased Alignment on Micropatterned Hydrogels Compared to Unpatterned Hydrogels

The nuclear angle of cells seeded on hydrogels were assessed with a model myoblast cell type, C2C12 murine myoblasts. In Figure 14B, the percent of nuclear alignment with respect to the axis of the direction of the micropatterns is displayed. All micropatterned surfaces had statistically significant increases in nuclear alignment compared to the unpatterned control, 0 µm. In terms of the mean nuclear angle of each micropatterned group, Figure 14C showed average angles statistically lower than that of 0 µm. All micropatterned groups, except 100 µm, were statistically more aligned than 0 µm. Histogram of the distribution of the total number of cells in each binning group for C2C12 alignment can be seen in Appendix D.

The cytoskeletal phenotype was examined in Figure 15. There was random orientation shown in 0 µm, indicated by flattened cytoskeleton with no coherent common direction. Cytoskeleton visually showed more alignment in the direction of micropatterns, as seen in all micropatterned conditions. At the larger channel geometries, such as 25, 50, and 100 µm hydrogels, cytoskeleton was seen aligning towards the edges of the micropatterned channels; however, cells began to show random orientations similar to that of 0 µm in the middle of the micropatterned plateaus and widths.

5.2 Specific Aim 2: Determine topographic features that maximize hiPS-CM cellular morphology.

Once the scaffold was created, the effects of aligned topography of hiPS-CM were examined by measuring nuclear alignment and phenotypic staining. Sarcomeric α-actinin and connexin-43 were stained because of their roles in cell maturity and function, and vinculin

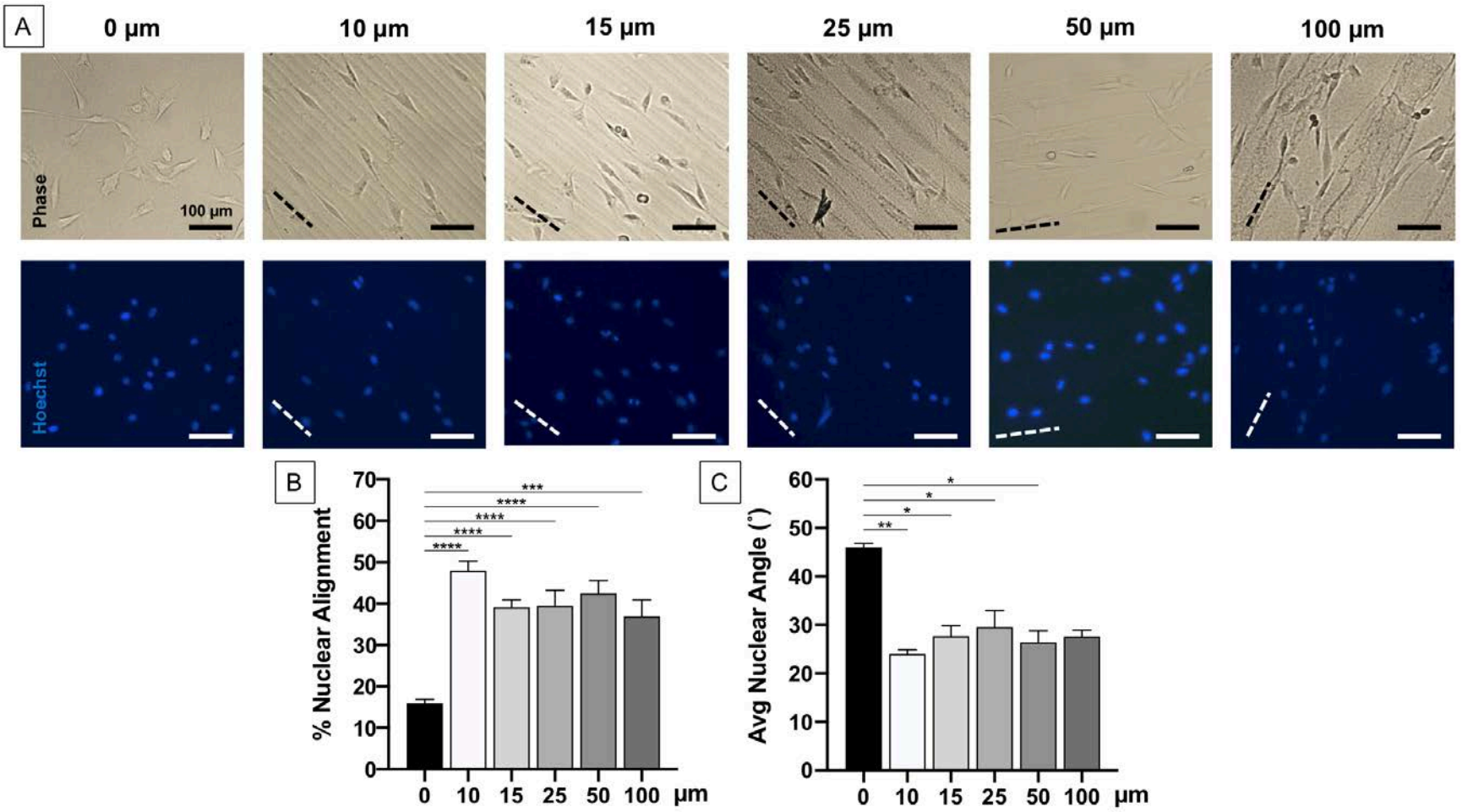

*Figure 14 (A) Representative phase and Hoechst images of C2C12 seeded micropatterned hydrogels. Dotted lines denote micropattern direction. (B) Percent alignment of C2C12 nuclei with respect to the direction of the micropatterned surface. Alignment is defined as falling within 15˚ of the axis. (C) The average angle of C2C12 nuclei was examined, with 0˚ indicating perfect alignment. Mean±SEM. Normality was determined with Shapiro-Wilk test, and one-way ANOVA with Tukey post-hoc analysis was performed in the case of normally distributed data (A), while a Kruskal-Wallis test with Dunn's multiple comparison was performed for nonparametric data (B). A bar represents significant difference, $p<0.0332$ for *, $p<0.0021$ for **, $p<0.0002$ for ***, $p<0.0001$ for ****. $N \geq 6$. ~125 cells/image were analyzed.*

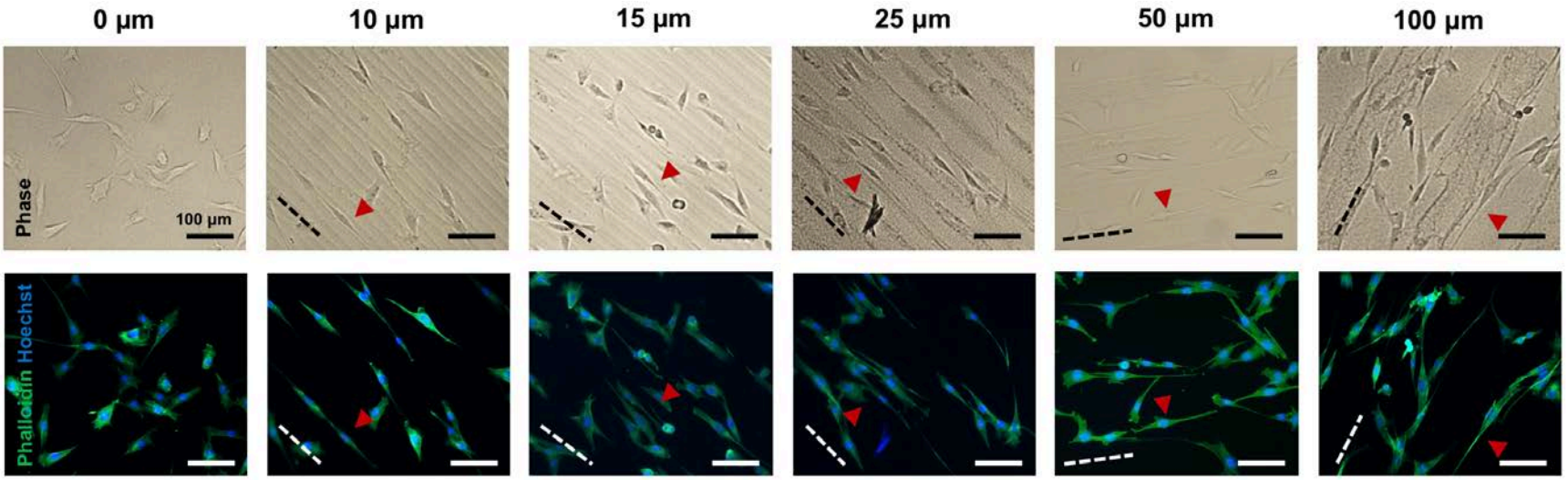

Figure 15 Phenotypic comparison of C2C12 cytoskeleton on micropatterned hydrogels. Cytoskeleton visually aligning with micropatterned channels is labeled with red arrows. Dotted lines denote micropattern direction.

was examined because of its role in gap junction formation and ability to depict directionality [90].

5.2.1 hiPS-CM Have Increased Nuclear Alignment on Micropatterned Hydrogels

The nuclear orientation was examined for hiPS-CM seeded coverslips and 0, 10, and 100 µm hydrogels in Figure 16A. A 2D coverslip (CS) was used as a control for hiPS-CMs. Only the 10 µm and 100 µm micropatterned hydrogels were chosen for hiPS-CM culture in order to compare the different effects on opposite ends of the micropatterned spectrum.

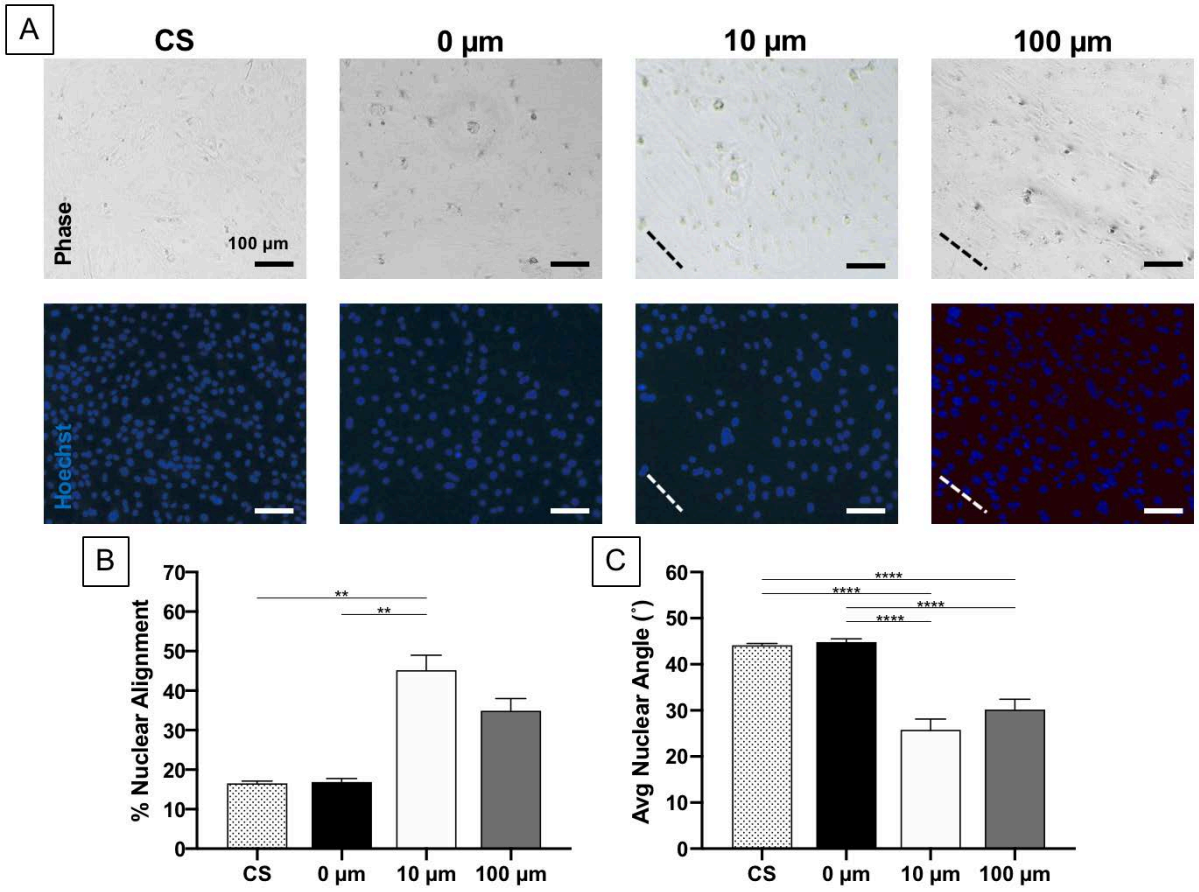

*Figure 16 (A) Representative phase and Hoechst images of hiPS-CM seeded coverslips and 0 µm, 10 µm, and 100 µm hydrogels. Dotted lines represent micropattern direction. (B) Percent alignment of hiPS-CM nuclei with respect to the direction of the micropatterned surface. Alignment is defined as falling within 15˚ of the axis. (C) The average angle of hiPS-CM nuclei was examined, with 0˚ indicating perfect alignment. Mean±SEM. Normality was determined with Shapiro-Wilk test. A Kruskal-Wallis test with Dunn's multiple comparison was performed for nonparametric data (A), and a one-way ANOVA with Tukey post-hoc analysis was performed in the case of normally distributed data (B). A bar represents significant difference, $p<0.0021$ for **, $p<0.0001$ for ****. $N \geq 5$. ~300 cells/image were analyzed.*

In Figure 16B, only the 10 μm hydrogels were more aligned compared to the coverslip and 0 μm hydrogel controls. In Figure 16C, both the average angles of 10 and 100 μm hydrogels were statistically different to the coverslip and 0 μm controls. Histogram of the distribution of the total number of cells in each binning group for hiPS-CM alignment can be seen in Appendix E.

5.2.2 Connexin-43 Expression Indicates Maturation with Extended Culture Periods

Markers of mature cardiomyocyte phenotype, sarcomeric α-actinin and connexin-43, are examined in Figure 17 for hiPS-CM seeded constructs cultured for 7 and 14 days. Striated actinin can be seen in all conditions at both time points, indicating functional, contracting cells. Connexin-43 is present in circumferential morphology in Day 7 constructs for some conditions, indicating the beginnings of mature gap junction formation. At Day 14, more circumferential connexin-43 staining is observed in all conditions, and the micropatterned hydrogels display more expression compared to the 0 μm constructs. hiPS-CM seeded on micropatterned hydrogels displayed a strong lateral connexin-43 staining parallel to channel direction. Additionally, actinin staining was used to characterize cytoskeletal morphology in Figure 17. Flat, rounded extracellular shape is seen in the coverslip and 0 μm conditions, while more elongated morphology in the direction of patterning is seen in the micropatterned hydrogels. As seen with C2C12s in Figure 15, in hiPS-CM in Figure 17 begin to display wide, flat morphology in the 100 μm hydrogels on the plateaus and widths but still show some directionality along the micropatterned edges similar to morphology seen in the 10 μm hydrogels. Positive and negative controls can be seen in Appendix F.

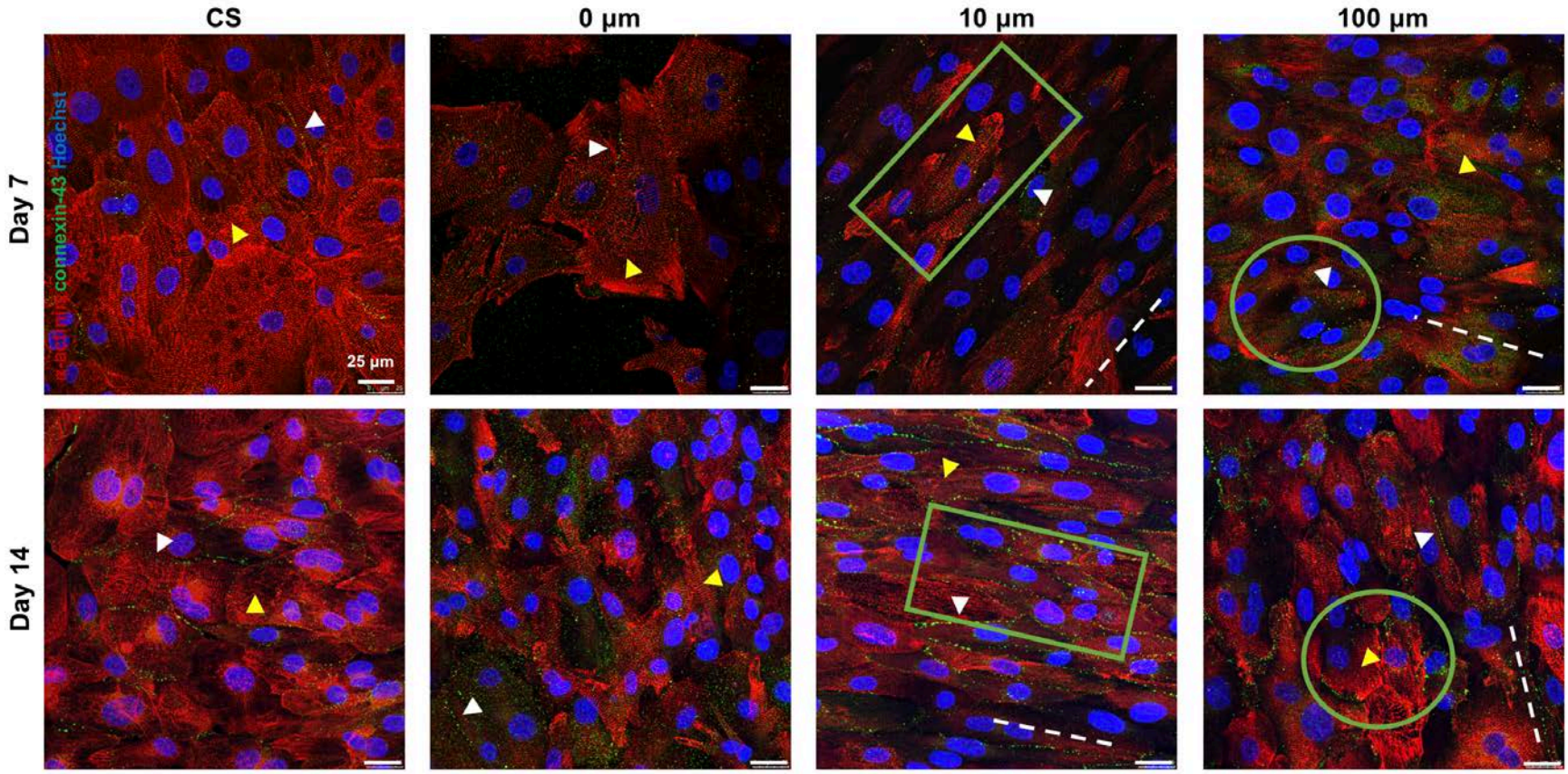

Figure 17 Phenotypic analysis of hiPS-CM seeded constructs at Day 7 (top) and Day 14 (bottom) in representative images. At Days 7 and 14, mature, striated sarcomeric α-actinin is present (yellow arrows). In Day 7, little circumferential connexin-43 is present (white arrows). At Day 14, more circumferential connexin-43 is prevalent in all samples and is pronounced in the 10 and 100 µm micropatterned hydrogels. Flat morphology similar to that of the unpatterned controls is seen in 100 µm hydrogels (green circles), but elongated cell morphology is present in 10 µm hydrogels (green rectangles). Dotted lines denote micropattern direction.

5.2.3 Vinculin Staining Does Not Indicate Cell Directionality in hiPS-CM Seeded Hydrogels

Focal adhesions were characterized in hiPS-CM seeded constructs in order to further characterize cellular alignment [90]. Vinculin was chosen because of its role in connexin-43 signaling [91]. As seen in Figure 18, characteristic punctate vinculin staining on the outer edges of the cytoskeleton is only observed in the coverslip control. In the 0, 10, and 100 µm

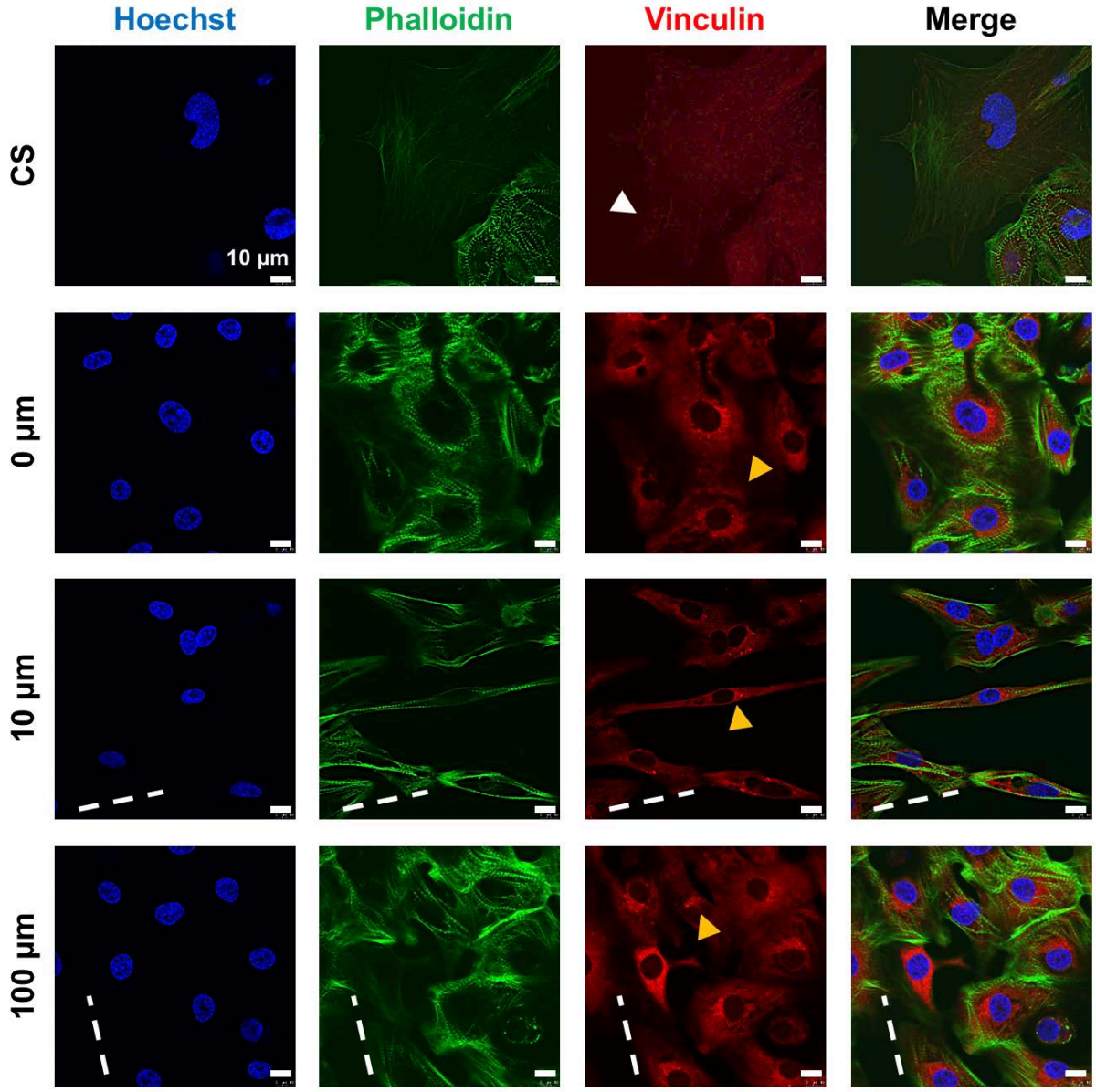

Figure 18 Analysis of vinculin morphology with respect to phalloidin and Hoechst on hiPS-CM cultured for 2 days. Punctate vinculin staining is only visible towards the outer bounds of the cytoskeletal in the coverslip control (white arrow), while random vinculin scattering is observed throughout the cells and congregated near the nucleus for all hydrogel conditions (yellow arrows). Dotted lines denote micropattern direction.

hydrogels, vinculin staining is observed scattered throughout the cell-construct interface and concentrated especially at the nucleus. Due to the scattering morphology, cell directionality could not be estimated in the micropatterned hydrogels. Negative controls can be seen in Appendix G.

5.3 Specific Aim 3: Characterize the contractile strain response of hiPS-CM seeded micropatterns to electrical stimulation.

In this final aim, the contractile strain of hiPS-CM seeded micropatterned hydrogels will be examined when cultured with and without electrical stimulation using HDM.

5.3.1 Micropatterning and Electrical Stimulation Display Higher Contractile Strains

hiPS-CM seeded constructs were cultured under continuous electrical stimulation for 7 days to determine the effects electrical stimulation have on contractile strain. After 7 days, high-speed videos were taken of each construct and HDM was performed to measure the contractile strain of each condition. Contractile HDM videos of all conditions can be seen Figure 19B. Figure 20A shows the average contractile strain was greater in the micropatterned hydrogels compared to coverslip controls, but only the 10 µm hydrogels

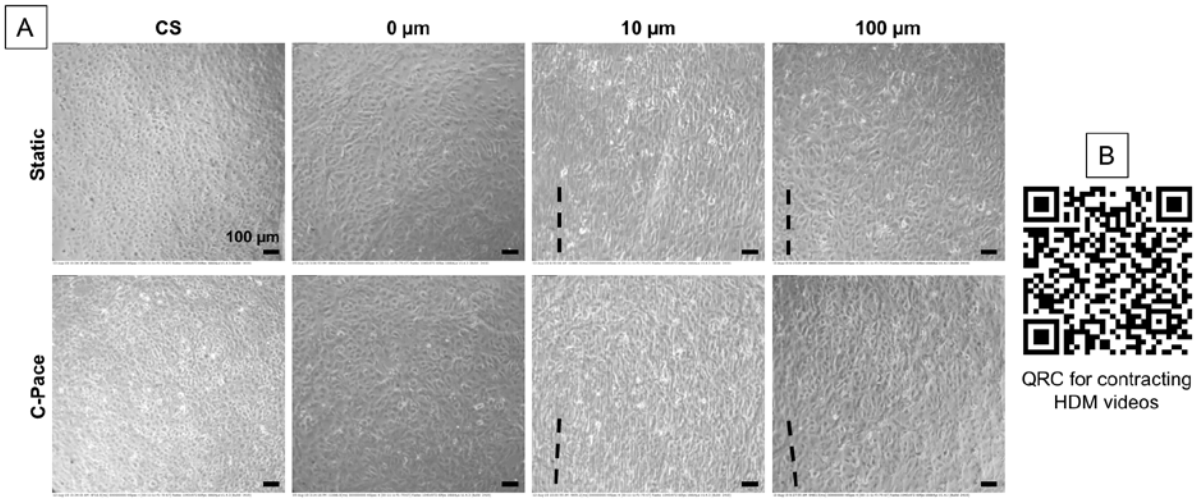

Figure 19 (A) Still images of phase high-speed videos of contracting hiPS-CM seeded coverslips and 0 µm, 10 µm, and 100 µm hydrogels. Dotted lines denote micropattern direction. (B) QRC link to contractile HDM videos for Static and C-Pace culture of coverslip and 0, 10, and 100 µm hydrogels.

cultured under electrical stimulation were statistically different from the 0 µm control. The same trend was observed for the maximum contractile strain observed per condition, shown in Figure 20B.

Phenotypic differences were compared between static culture (Figure 20) and electrical stimulation culture (Appendix H). Samples displayed no clear differences in sarcomeric structure or connexin-43 expression at Day 7 or Day 14 time points. Cell elongation was not different between static culture and electrical stimulation culture hiPS-CM seeded hydrogels, and there was no difference in nuclear alignment (Appendix I).

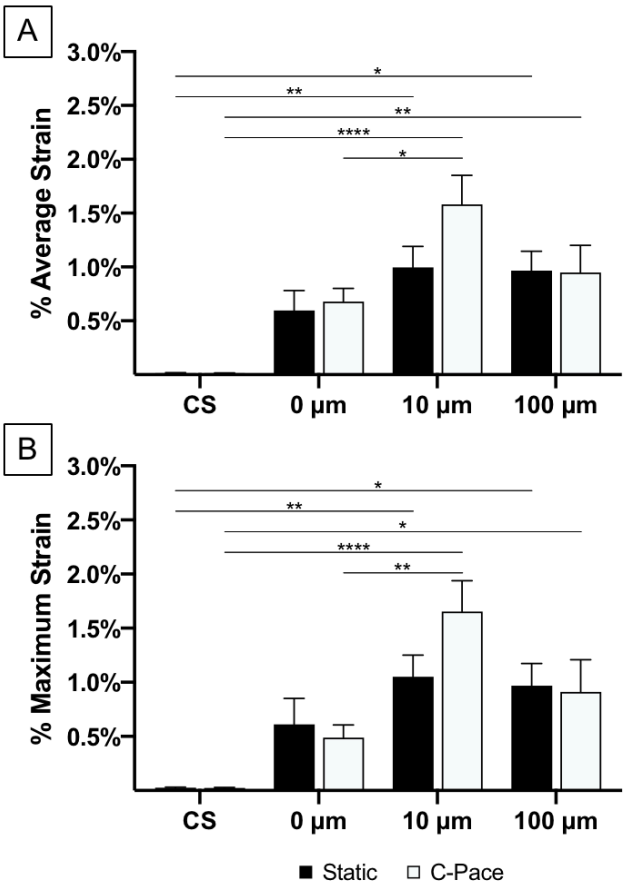

*Figure 20 Using HDM, the percent average contractile strain (A) and the percent maximum contractile strain (B) of hiPS-CM seeded constructs were examined when cultured under continuous electric stimulation using C-Pace for 7 days compared to static, no stimulation culture. Mean±SEM. Normality was determined with Shapiro-Wilk test, and a two-way ANOVA with Sidak post-hoc analysis was performed. A bar represents significant difference, $p<0.0332$ for *, $p<0.0021$ for **, $p<0.0002$ for ***, $p<0.0001$ for ****. $N \geq 6$.*

Chapter 6 Discussion

The long-term goal of this project is to design an implantable, contractile cardiac patch to be used as a functional replacement of ventricular myocardium in the event of heart failure following an MI. The only current long-term treatment available for heart failure is whole-organ heart transplant [1]. In the event ventricular dilation, the use of a cardiac patch can be implanted with SVR to reshape the tissue and to restore some function in the case of myocardial thinning. Current cardiac patches are made of synthetic materials or porcine pericardium and have been shown to illicit a fibrous encapsulation at site of implantation [5]. Additionally, these are acellular materials that lack the functionality that comes from a contractile cellular environment [32]. Our lab has previously used the natural biomaterial fibrin to create a cardiac patch with mechanical properties similar to native myocardium [78]. hiPS-CM have the potential to be patient specific, avoiding immunological response to foreign cells. We propose the use of the natural biomaterial fibrin in combination with hiPS-CM to prevent an immunological response that would promote integration into the native myocardium [10]. Micropatterned fibrin scaffolds were developed to increase alignment of hiPS-CM and could be used to match native architecture and functional properties. Scaffold morphology was characterized through bright field and confocal imaging for the PDMS negative replicates as well as micropatterned hydrogels. An increase in nuclear alignment was shown for two cell types, and the hiPS-CM phenotype was determined through markers for maturity as well as adhesion to the material. Constructs were cultured under electrical stimulation in order to assess the effects of electrical stimulation on contractile strain, which was determined using HDM, and demonstrated that micropatterned hydrogels had increased contractile strain compared to unpatterned controls.

6.1 Specific Aim 1: Develop fibrin scaffolds with aligned surfaces to increase nuclear orientation.

6.1.1 PDMS Photolithography Allows for the Fabrication of Micropatterned Hydrogels

Photolithography has been used numerous times to impart microscale topographies in scaffolds (Table 1). Previous groups have encouraged cell alignment on topographical features and transferred aligned cells to fibrin hydrogels to create anisotopically aligned constructs [92, 93]. The novel technology of altering the surface of a fibrin hydrogel to in linear, channel geometry through micropatterning has created a facile method of aligning cardiomyocytes and encouraging increased contractile strain. Future work in surface characterization can be performed using atomic force microscopy (AFM) to determine the modulus of the hydrogel [94].

6.1.2 Micropatterned Hydrogels Retain Channel Geometry and a Reliable Replication of Micropattern Depth

The micropatterned hydrogel conformed to similar topographical geometry from the PDMS negative replicates. Sectioning the PDMS and imaging with bright field microscopy was sufficient for measuring the plateau, width, and depth. Hydrogels were dip-coated in rhodamine dye in PBS, and rhodamine binds to the fibrin through electrostatic forces, allowing the hydrogel to be fluorescently imaged. These images were then exported in the orthogonal view and measured in the same manner as the PDMS negative replicates.

Confocal imaging hydrogels provided a more accurate representation than sectioning as the sectioning process caused shrinkage and distortion of the hydrogel geometry (Appendix C). The process did provide, however, evidence of patterning. Rhodamine dying

the hydrogels and imaging with a confocal microscope allowed for a more accurate representation of the hydrogel.

All micropatterned hydrogels except the 10 µm hydrogel had smaller plateaus and widths than the PDMS negative replicates, and all hydrogels displayed a depth of 0.3 that of PDMS negative replicate. This relationship can be utilized in future design of channel geometry in fibrin hydrogels for additional applications in addition to cardiac patches, such as skeletal muscle or the microenvironment necessary for epithelization of skin applications [85].

6.1.3 C2C12 Nuclei Have Increased Alignment on Micropatterned Hydrogels Compared to Unpatterned Hydrogels

In the initial assessment of nuclear angle, cells on all micropatterned hydrogels had increased nuclear alignment except the largest, 100 µm, had decreased mean angles compared to an unpatterned hydrogel control. C2C12s were used as facile myoblast model to hiPS-CM for initial cell alignment. They were seeded at a lower cell density to better assess the effects micropatterning has on cellular orientation.

Micropatterning used for skeletal and cardiac muscle alignment has shown high degrees of cellular alignment in micropatterns displaying a range of channel geometries from 1 – 50 µm and depths of 1 – 25 µm [65, 92, 95, 96]. Generally, cellular alignment was greatest in samples that had channel geometries ~10 µm and depths greater than 5 µm. Channel geometry needed to be distinct enough to encourage cell alignment but not so small as to be negligible for contact guidance. Additionally, larger geometries discouraged cellular alignment with a similar pattern of negligible contact guidance in expansive, flat geometries.

All micropatterned samples seeded with C2C12s had increased nuclear orientation compared to the unpatterned hydrogel. When it came to the mean nuclear angle, all micropatterned hydrogels except the 100 μm hydrogels depicted mean angles statistically less than that of the unpatterned control. Both metrics did not show statistical significance in alignment between micropatterned conditions.

In order to assess any differences between geometries, the cytoskeletal phenotype was examined in Figure 15. Directionality of the cytoskeleton was not measured because of planar differences in imaging; however, it can depict trends in cellular alignment [56]. When examining the cytoskeletal morphology, areas of random orientation were present more often as the micropattern geometry increased in channel size. Cells were aligned along the edges of the widths and plateaus, which would account for the increase in nuclear alignment seen in Figure 14.

It is of note that cells displayed a nuclear alignment of 47.9% and an average angle of 24.1˚ in the 10 μm hydrogels. Nuclei in human myocardium aligns at 46% and has an average angle of 25.7˚, indicating cells seeded on the 10 μm hydrogel were closest to native myocardium architecture [97]. The other micropatterned hydrogels, with the exception of the 100 μm hydrogels, displayed little to no statistical differences between micropatterned groups but morphological evidence of a difference in cellular behavior. Because the 10 μm patterned hydrogels resemble native myocardium and the 100 μm hydrogels exhibit different alignment and phenotype, only the 10 μm and 100 μm hydrogels were selected to investigate by incorporating hiPS-CM into the system.

6.2 Specific Aim 2: Determine topographic features that maximize hiPS-CM cellular morphology.

6.2.1 hiPS-CM Have Increased Nuclear Alignment on Micropatterned Hydrogels

Verification of the ability of micropatterned hydrogels to align hiPS-CM determined similar trends for aligning hiPS-CM as C2C12s. While C2C12s work as a model system because of myoblasts need for alignment when forming myotubes, an initial verification of hiPS-CM alignment was required. hiPS-CM seeded on 0, 10, and 100 μm hydrogels (Figure 16) had similar percent nuclear orientation and average angle values to C2C12 seeded scaffolds (Figure 14).

The coverslip and 0 μm hydrogel controls had statistically similar orientation patterns as well. The percent nuclear alignment was less than 20% for both, and the average nuclear angles were ~45˚. Both these parameters indicate random cellular alignment. As the histogram for nuclear alignment bins with 15˚ increments, ~20% falling in every bin group from 0˚ to 90˚ indicates random orientation. By the same principle, the average angle falling at ~45˚ also indicates random alignment.

Based on both parameters used to measure alignment in Figure 16, both micropatterned surfaces increased nuclear alignment for hiPS-CM. The increase in alignment for 100 μm hydrogels could be due to the extended culture time to achieve better maturation and attachment necessary for hiPS-CM [83, 98].

6.2.2 Connexin-43 Expression Indicates Maturation with Extended Culture Periods

hiPS-CM were cultured on coverslips and 0, 10, and 100 μm hydrogels for 7 and 14 days before staining for sarcomeric α-actinin and connexin-43. Distinct, regularly spaced sarcomere Z-bands were visible at Day 7 and 14 in all samples. Higher magnification or

alternative staining would need to be performed in order to identify other sarcomeric structures, such as A-, I-, or M-bands, which indicate later stages of hiPS-CM maturation [11]. Nevertheless, the presence of the organized, elongated, and distinctly spaced sarcomeres indicate the hiPS-CM are in later stages of differentiation and are behaving closer to adult cardiomyocytes than fetal ones (Figure 9) [98, 99].

Connexin-43 staining was visible between cells in small quantities starting on Day 7 but was greatly increased to circumferential patterns at Day 14. Some punctate staining scattered throughout the cell is seen in Day 14 coverslips, which also indicates immature staining; however, this was observed in numerous locations within hydrogels where there were no cells present [9]. Due to autofluorescence of fibrin, we cannot determine if this staining is present in all samples. Connexin-43 is essential in gap junction formation, and a more mature phenotype would display connexin-43 at the polar ends of an elongated cell, as illustrated in Figure 9. The increase in staining at the cellular boarders between time points suggests that cell maturation continues to occur over time. Polar connexin-43 has been known to occur in later stages of hiPS-CM maturation and usually expressive in systems that also demonstrate electrical coupling or are cultured in the presence of fibroblasts. For increased connexin-43 expression, we would suggest culturing our hiPS-CM seeded constructs with the addition of cardiac fibroblasts, as discussed in Section 7.2 Introduction of Fibrin Microthreads and Cardiac Fibroblasts through Co-Culture System.

6.2.3 Vinculin Staining Does Not Indicate Cell Directionality in hiPS-CM Seeded Hydrogels

Punctate vinculin staining was seen in coverslips but not hydrogel conditions. Focal adhesions couple actin to the transmembrane, and these proteins are necessary in the cellular pathway that regulates cell remodeling and response to cardiac hypertrophy [9]. Intercalated

discs (ICDs) are composed of adherens junctions, desmosomes, and gap junctions. Adherens junctions and desmosomes are responsible for cell-cell coupling and mechanical integration, while gap junctions are responsible for electrical continuity [100]. Vinculin, a protein associated with adherens junctions, is responsible for determining cell shape and alignment [91, 100]. Additionally, it has been shown to be responsible to stabilize connexin-43 gap junctions by interacting with the protein family responsible for these cell-cell junctions [91]. Connexin-43 directly interacts with zonula occludens-1 (ZO-1) which is part of the zonula occludens family that is responsible for tight junctions and adherens junctions. In cardiomyocytes, ZO-1 and connexin-43 congregate at the ICDs. Vinculin directly interacts with ZO-1, and the loss of vinculin results in the loss of ZO-1 and thus connexin-43 in an area. Punctate vinculin staining showing cell directionality and shape is indicative of connexin-43 presence [90, 91]. Because of this important role in cardiomyocyte contractility, we looked to examine its phenotype with respect to micropatterned hydrogels and cellular alignment [90].

When examining the vinculin staining patterns, only the coverslip control expressed punctate, distinct staining: all hydrogel conditions showed vinculin spread throughout the cell. The diffuse pattern shown throughout the cell interface is not characteristic of a 3D micropatterned substrate but is of a softer cell scaffold [101]. Because of vinculin's role in mechanical force, it is possible that the 10 mg/mL fibrin hydrogel at ~0.5-1.2 kPa is too soft to promote punctate staining. To maintain the concept of a contractile surface but also show punctate staining that could indicate cell directionality, a stiffer fibrin hydrogel that could deform with contractions would be required, as explored in Section 7.5 Verification of Vinculin Staining as a Function of Stiffness [101, 102].

6.3 Specific Aim 3: Characterize the contractile strain response of hiPS-CM seeded micropatterns to electrical stimulation.

6.3.1 Micropatterning and Electrical Stimulation Display Higher Contractile Strains

Through HDM analysis and strain calculations, a combination of micropatterning and electrical stimulation increased contractile strains. Electrical stimulation did not increase strain rates within each construct condition. Both the 10 µm and 100 µm hydrogels had statistically larger average strains and maximum strains than the coverslips for static and paced cultured samples; however, there were no differences in strain rate between the static cultured hydrogels. The main difference was observed when the 10 µm hydrogels displayed higher contractile strains than the 0 µm hydrogels only when cultured with electrical stimulation.

hiPS-CM spontaneously beat when there are nodal, or pacemaker, cells present in the cell population; otherwise, hiPS-CM will only beat with electrical stimulation inducing electrical pulses to the system [103, 104]. CDI's iCell Cardiomyocyte^2 have noted a small percentage of the population to be non-cardiomyocyte, and with spontaneous beating, the presence of nodal cells is indicated to be a part of this small percentage [83]. By conditioning the hiPS-CM through electrical stimulation, the addition of electrical stimulation to the system allows for conditioning for synchronized contractions, which leads to greater contractile force or strain and decreased calcium handling times necessary for mature cardiac tissue [104].

Electrical stimulation in culture can lead to increased maturity in hiPS-CM and has been shown to increase maturity in sarcomere structure and connexin-43 expression [9]. When comparing the phenotype of 7 and 14 days of culture in static samples (Figure 17) and

C-Pace cultured samples (Appendix H), there is no clear structural differences between sarcomeric structure and connexin-43 expression. Additional microscopy techniques, such as transmission electron microscopy, could be used to see other sarcomere structures indicative of maturity or render a 3D projection allowing for complete z-bands that could be measured and compared [11].

To increase cell maturity, an alternative protocol electrical stimulation and prolonged culture times should be examined next in this system. It is generally agreed upon that prolonged culture times greater than 14 days will result in more mature cardiomyocyte sarcomere phenotype, and prolonged culture with cardiac fibroblasts will result in a more polarized connexin-43 expression [11, 45]. Combining increased culture time with alternative electrical stimulation protocols can also yield mature contractile properties of hiPS-CM as well. Long term culture subjected to intensity training through steadily increasing stimulation frequency has been shown to mature hiPS-CM in 21 days [105].

There were no alignment differences between static and electrically cultured hiPS-CM seeded hydrogels (Appendix I). The same trend is observed in both the percent nuclear alignment as well as the average nuclear angle, and elongated cellular shape is similar in the static and electrically cultured samples. In this case, the micropatterned topography took a higher presidency in aligning cardiomyocytes than electrical stimulation would have [72].

As can be seen in the contracting videos in Figure 20B, there are regions that contract at different frequencies within each ROI. As nodal cells may be the source of contractions in those videos, surrounding areas received different electrical input at Day 7 and the contractile regions were not synchronized to one uniform system after 7 days of continuous electrical stimulation. One way of characterizing these changes is through small region HDM, in which

20 small regions over the video are analyzed for differences in frequency and contractile strain [97]. By predetermined parameters, such as the use of IQR, outliers in contractile strain could be eliminated from the whole. In large region HDM performed here, the differences in frequency over the ROI is an indication that the system has not begun to beat synchronously after 7 days of stimulation [105, 106]. Synchronous beating could be obtained by altering the pacing protocol waveform, culture time, or gradually increasing frequency over an extended culture time.

Of note, the contractile strains measurements are low compared to native ventricular myocytes. In the human left ventricle, strain values have been measured at ~23-30%, and hiPS-CM contractile strains on a 3D scaffold for 7 days have been recorded at ~3.5% [107-109]. HDM was originally developed as a particle-tracking algorithm to measure contractile strains on *in vivo* cardiac tissue [88]. Additionally, it has been shown to measure contractile strains in other *in vitro* 3D cardiomyocyte constructs [86, 87]. In our constructs, however, hiPS-CM contractions can go out of frame (Figure 20B), causing loss of information as each pixel's true trajectory is cut short before the end of the contraction, reporting a lower contractile strain rate. Contractile strain measurements through HDM may be more accurate when analyzing multiple patches laminated to the specifications of 3D myocardial tissue. Future HDM will be analyzed on recordings imaged at a lower magnification to capture complete contractions. Additionally, an increase in contractile strain may be observed by analyzing the principal strain. By calculating principal contractile strain with the principle angle contraction, there could be an increase in contractile strain of aligned hiPS-CM on micropatterned scaffolds. Future HDM assessment will characterize principal contractile strains and strain angles.

Chapter 7 Future Works and Recommendations

There are several recommendations outlines below for the future of this project. Additional measurements to quantify contractile output are examined, as well as additional methods to culture and advance the micropatterned fibrin hydrogel.

7.1 Measuring Contractile Wave Propagation via Calcium Imaging

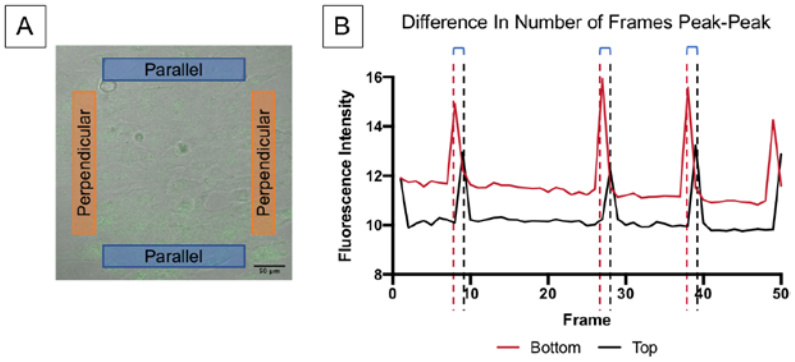

Figure 21 (A) Videos of contracting micropatterned hydrogels labeled with Calcium Green are tracked as the wave travels from the bottom to the top of frame parallel to the channels as well as perpendicular. (B) The difference in the number of frames between the wave reaching each ROI is determined graphically.

Additional experimentation on the difference in contractile wave propagation could be measured through the use of calcium imaging. By using a cell permeant, such as Calcium Green (Invitrogen) or Fluo-4 AM (Thermo Fisher Scientific), to fluorescently label calcium transits in the cells, high-speed videos could be obtained of the wave propagation [110]. Bright field imaging is used to confirm mechanical contraction [87]. Initial experimentation was performed using this technique, as outlined below.

To visualize calcium transients, cells were permeated with Calcium Green and imaged at 25× using a Zeiss LSM 510 meta microscope (Zeiss, Thornwood, NY, USA). As outlined in Figure 21, calcium green was tracked as it travels between two ROIs: parallel and perpendicular to the micropatterned channels. The difference between frames was then determined graphically using the fluorescence intensity of the ROIs. This difference in

frames was then multiplied by the recording frame rate, and this resulting value was divided by the distance between the two ROIs to give the contractile wave propagation speed.

Videos of calcium green contracting hiPS-CM can be seen in Figure 22B, and the contractile wave propagation speed for the coverslip and 10 µm and 100 µm hydrogels are shown in Figure 22C. Propagation speeds were measured at ~33 µm/s for both directions, while propagation speeds for human myocardium is closer to 73±4 cm/s in the longitudinal direction and 11±3 cm/s in the transverse direction [111]. This slower wave propagation speed can be indicative of immature calcium transportation; however, because the frame rate was set to 9 fps, differences in propagation speed are difficult to measure between frames, and imaging would need to be performed with a higher speed camera in order to best understand calcium transient activity.

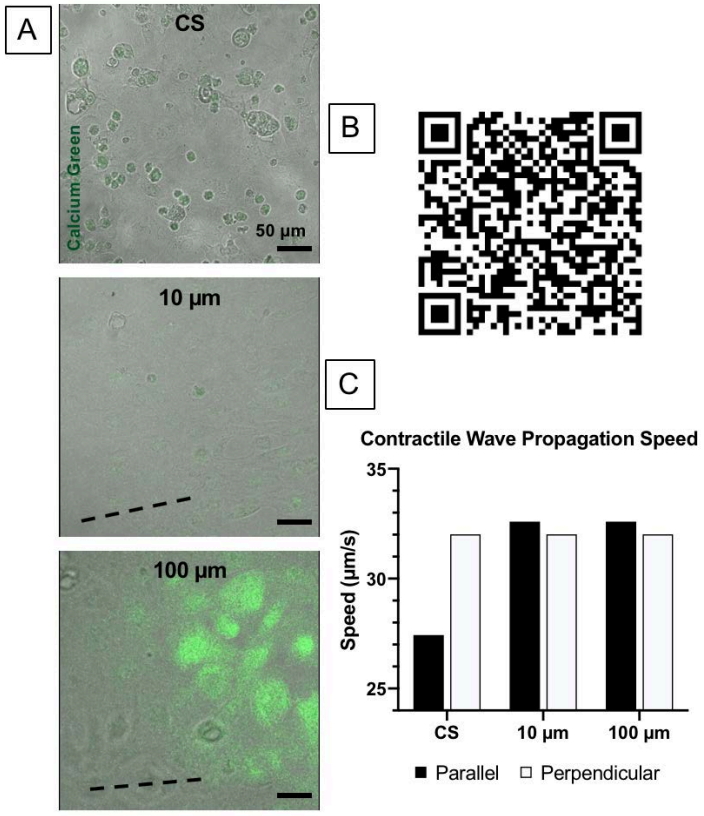

Figure 22 (A) Still images of calcium green imaging for coverslip and 10 µm and 100 µm hydrogels. Dotted lines denote micropattern direction. (B) QRC code to calcium green labeled contractile videos. (B) Contractile wave propagation speeds for the coverslip and 10 µm and 100 µm hydrogels in the parallel and perpendicular directions. While there is no directionality on the coverslips, these ROI are consistent to the micropatterned hydrogel ROIs.

7.2 Introduction of Fibrin Microthreads and Cardiac Fibroblasts through Co-Culture System

The addition of cardiac fibroblasts to hiPS-CM culture has been shown to be beneficial to cardiomyocyte maturation and electrical signal propagation by allowing for increased contractile wave propagation, increased contractile force, and increased contractile velocity compared to cardiomyocytes cultured alone [15, 17]. As cardiac fibroblasts make up the majority of cells in the myocardium, their role in mimicking left ventricle architecture is necessary in addition to cardiomyocytes.

As shown in Figure 23, a proposed co-culture design would incorporate the use of a micropatterned composite fibrin microthread and hydrogel cardiac patch. We showed that microthreads can be incorporated into micropatterned hydrogels (Appendix C). With the addition of cells, we would expect fibroblasts to align under anisotropic tension in the base of the fibrin microthreads, and cardiomyocytes seeded on the micropatterned surface of the hydrogel to display increased cellular alignment as demonstrated in this thesis. By utilizing calcium imaging in this co-culture method, we would expect a reduction in calcium transient time and an increase in action potential duration, as characteristic in mature cardiac tissue [112]. As previously demonstrated with rNVM seeded composite patches, laminating multiple patches would produce a cardiac patch with physiologically relevant thickness to the myocardium [86]. This co-culture system would advance the design and functionality of our engineered cardiac patch.

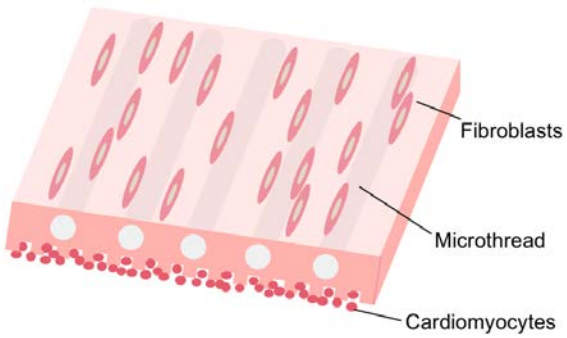

Figure 23 Schematic of co-cultured system of a micropatterned composite fibrin microthread and hydrogel cardiac patch. Alignment of cardiac fibroblasts occurs in the hydrogel-microthread fraction of the patch, and alignment of cardiomyocytes occurs through micropatterning.

7.3 Introduction of a Vascular Network

Oxygen diffusion is limited to within 200 µm of a vascular network, and the lamination of fibroblast-cardiomyocyte layers to a physiologically relevant thickness of ~1.5 cm would require the addition of vascular networks within the layers of the tissue engineered construct [32, 113]. Our lab has previously shown the addition of a fibrin-based mesovascular network to the Composite Cardiac Patch allowed for diffusion of calcein AM to cells ~200 µm from the vasculature [86, 114]. Additionally, the use of a decellularized spinach leaf as a microvascular network could be used in combination with a fibrin cardiac patch in order to increase cardiomyocyte alignment as well as offer a vascular supply to cells [113]. Either option could be confirmed for functionality by first perfusing calcein AM through the vasculature to check for cellular uptake and advanced by endothelializing the vascular lumens. Eventual implantation of the patch would involve connecting the tissue engineering vasculature to native tissue vasculature to ensure survival of the implanted cells.

7.4 Mechanical Stimulation of Cultured Cardiac Patches

In addition to increasing cardiomyocyte alignment, mechanical stimulation can increase

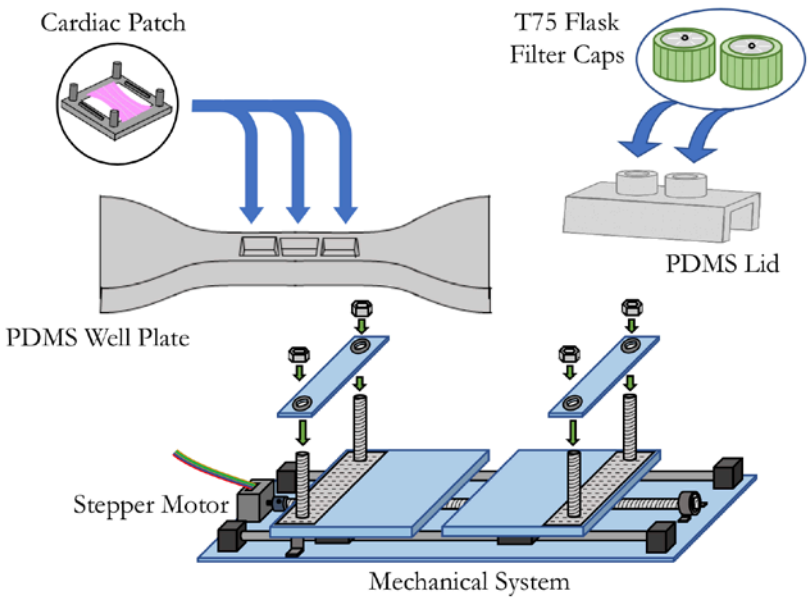

Figure 24 Mechanical stimulator designed for the Composite Cardiac Patch, involving a custom PDMS well plate in the dog-bone shape used in tensile testing. A custom PDMS lid allows for motion of the well plate, and a stepper motor causes movement of the mechanical system and thus the well plate.

Source: Cerkanowicz D, Conlen M, Ghahremani S, and Rosenthal A. "Design of a Biomimetic Mechanical Stimulator for Engineered Myocardium." 2019. WPI MQP.

maturity in cardiomyocytes [104]. As the heart develops from fetal to adult myocardium, contraction and shear forces influence cardiomyocyte development through cell shape and elongation. In mature myocardium, abnormal mechanical forces stimulate signaling pathways that trigger cardiac hypertrophy. When mechanical stimulation occurs through dynamic stretch, cardiomyocytes can be conditioned to undergo maturation. hiPS-CM have been shown to have increased sarcomere organization, leading to increased action potential durations and upstroke velocity [9].

Our lab has developed a mechanical stimulator designed to uniaxially stimulate the Composite Cardiac Patch, as seen in Figure 24 [115]. A custom PDMS dog-bone-shaped well plate was created to be used in the mechanical stimulator that was controlled by a stepper motor. This mechanical stimulator showed increased cytoskeletal alignment in a C2C12 seeded cardiac patch when cultured under cyclic stretch at 5-15% strain for 6 days under a duty cycle of 1 hr stimulation, 5 hr rest (Figure 25). Additional steps for this stimulator would be to culture a composite micropatterned patch with cardiomyocytes and measure contractile strain through HDM after 2 weeks of stimulation, as well as determine phenotypic differences in static and dynamic

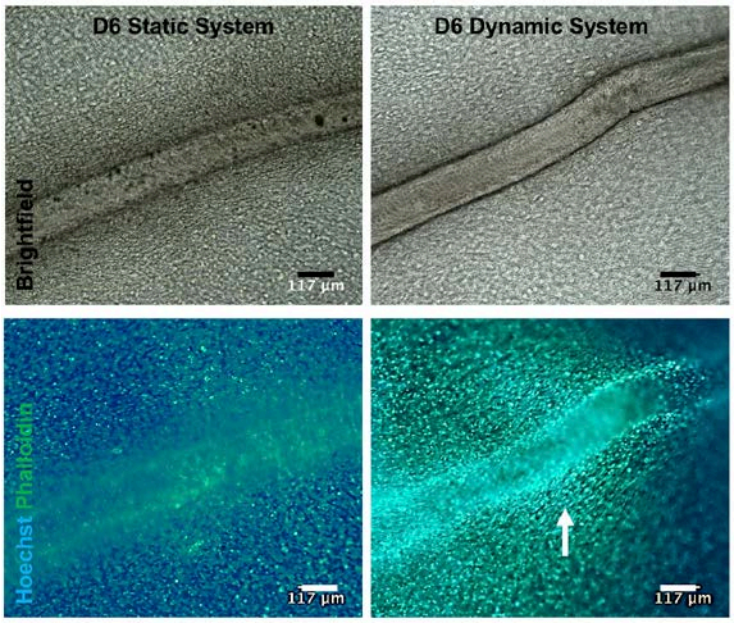

Figure 25 Images of Composite Cardiac Patches cultured for 6 days under static conditions (left) and mechanical stimulation (right). Alignment of cytoskeleton was present in the dynamic system (white arrow) that was not present in the static system within ~150 µm of the fibrin microthread.

Source: Cerkanowicz D, Conlen M, Ghahremani S, and Rosenthal A. "Design of a Biomimetic Mechanical Stimulator for Engineered Myocardium." 2019. WPI MQP.

culture through immunofluorescence.

7.5 Verification of Vinculin Staining as a Function of Stiffness

The lack of punctate vinculin staining on the hiPS-CM seeded on fibrin hydrogels needs to be examined as a function of stiffness. The relationship between substrate stiffness and cardiomyocyte maturation has previously been established in that cardiomyocytes mature best on substrates that match the mechanical properties of healthy myocardium [116, 117]. Embryonic cardiac tissue has a stiffness in the low kilopascals, while adult cardiac tissue has a stiffness of about 10 kPa during diastole [118]. Our patch has a stiffness that falls into the embryonic range (~0.5-1.2 kPa) [102]. By examining changes in hydrogel stiffness through changes in fibrinogen or thrombin concentration, we could expect to also see a better organization of sarcomeres, polarized connexin-43 staining, and changes in contractility associated with better gap junction formation [117]. Hydrogel stiffness can be characterized through mechanical testing, and we expect the presence of punctate vinculin staining that could be measured in ImageJ to show directionality of the cells [90]. Punctate vinculin staining pattern should be present at 48 hrs of culture but can also be examined after 7 days of culture to ensure full attachment and elongation of cells.

Chapter 8 Conclusions

We hypothesize that micropatterning fibrin hydrogels for the use of a cardiac patch will increase cardiomyocyte alignment that, and culturing under electrical stimulation will promote increased contractile strain compared to unpatterned control hydrogel. This was accomplished through the development of a micropatterned fibrin hydrogel by using photolithography to create micropatterned geometry that fibrin hydrogel conformed to during polymerization. After an initial alignment assessment, the micropatterned hydrogels were seeded with hiPS-CM to determine maturity phenotypes and vinculin patterns. Sarcomere structure was organized in hiPS-CMs, and connexin-43 staining showed an increase in mature phenotype over 14 days. The 10 µm micropatterned hydrogels cultured under electrical stimulation showed an increase in contractile strain compared to the unpatterned hydrogels compared to 100 µm hydrogels or static cultured conditions. It is the recommendation that this technology be used in a composite fibrin microthread and hydrogel cardiac patch to create a multilayered, co-cultured cardiac patch with increased cell alignment and the potential for increased contractile properties found through extended culture time of hiPS-CM in the presence of cardiac fibroblasts.

References

[1] E.J. Benjamin, P. Muntner, A. Alonso, M.S. Bittencourt, C.W. Callaway, A.P. Carson, A.M. Chamberlain, A.R. Chang, S. Cheng, S.R. Das, F.N. Delling, L. Djousse, M.S.V. Elkind, J.F. Ferguson, M. Fornage, L.C. Jordan, S.S. Khan, B.M. Kissela, K.L. Knutson, T.W. Kwan, D.T. Lackland, T.T. Lewis, J.H. Lichtman, C.T. Longenecker, M.S. Loop, P.L. Lutsey, S.S. Martin, K. Matsushita, A.E. Moran, M.E. Mussolino, M. O'Flaherty, A. Pandey, A.M. Perak, W.D. Rosamond, G.A. Roth, U.K.A. Sampson, G.M. Satou, E.B. Schroeder, S.H. Shah, N.L. Spartano, A. Stokes, D.L. Tirschwell, C.W. Tsao, M.P. Turakhia, L.B. VanWagner, J.T. Wilkins, S.S. Wong, S.S. Virani, E. American Heart Association Council on, C. Prevention Statistics, S. Stroke Statistics, Heart Disease and Stroke Statistics-2019 Update: A Report From the American Heart Association, Circulation 139(10) (2019) e56-e528.

[2] R.A. Hortensius, W.-H. Lin, B.M. Ogle, Chapter 1 - Cardiac Tissue Engineering: A Pathway for Repair, in: P.A. Iaizzo (Ed.), Engineering in Medicine: Advances and Challenges, Elsevier Inc, London, UK, 2019, pp. 3-33.

[3] G. Buckberg, C. Athanasuleas, J. Conte, Surgical ventricular restoration for the treatment of heart failure, Nat Rev Cardiol 9(12) (2012) 703-16.

[4] Z. Mosala Nezhad, A. Poncelet, C. Fervaille, P. Gianello, Comparing the Host Reaction to CorMatrix and Different Cardiac Patch Materials Implanted Subcutaneously in Growing Pigs, Thorac Cardiovasc Surg 67(1) (2019) 44-49.

[5] J.S. Woo, M.C. Fishbein, B. Reemtsen, Histologic examination of decellularized porcine intestinal submucosa extracellular matrix (CorMatrix) in pediatric congenital heart surgery, Cardiovasc Pathol 25(1) (2016) 12-7.

[6] P.V. Kochupura, E.U. Azeloglu, D.J. Kelly, S.V. Doronin, S.F. Badylak, I.B. Krukenkamp, I.S. Cohen, G.R. Gaudette, Tissue-engineered myocardial patch derived from extracellular matrix provides regional mechanical function, Circulation 112(9 Suppl) (2005) I144-9.

[7] K.A. Gerbin, X. Yang, C.E. Murry, K.L. Coulombe, Enhanced Electrical Integration of Engineered Human Myocardium via Intramyocardial versus Epicardial Delivery in Infarcted Rat Hearts, PLoS One 10(7) (2015) e0131446.

[8] C.P. Jackman, A.M. Ganapathi, H. Asfour, Y. Qian, B.W. Allen, Y.Z. Li, N. Bursac, Engineered cardiac tissue patch maintains structural and electrical properties after epicardial implantation, Biomaterials 159 (2018) 48-58.

[9] R. Zhu, A. Blazeski, E. Poon, K.D. Costa, L. Tung, K.R. Boheler, Physical developmental cues for the maturation of human pluripotent stem cell-derived cardiomyocytes, Stem Cell Res Ther 5(5) (2014) 117.

[10] M.C. Barsotti, F. Felice, A. Balbarini, R. Di Stefano, Fibrin as a scaffold for cardiac tissue engineering, Biotechnol Appl Bioc 58(5) (2011) 301-310.

[11] T. Kamakura, T. Makiyama, K. Sasaki, Y. Yoshida, Y. Wuriyanghai, J. Chen, T. Hattori, S. Ohno, T. Kita, M. Horie, S. Yamanaka, T. Kimura, Ultrastructural maturation of

human-induced pluripotent stem cell-derived cardiomyocytes in a long-term culture, Circ J 77(5) (2013) 1307-14.
[12] R.M. Berne, B.M. Koeppen, B.A. Stanton, Berne & Levy physiology, 6th ed., Mosby/Elsevier, Philadelphia, PA, 2010.
[13] I.J. LeGrice, B.H. Smaill, L.Z. Chai, S.G. Edgar, J.B. Gavin, P.J. Hunter, Laminar structure of the heart: ventricular myocyte arrangement and connective tissue architecture in the dog, Am J Physiol 269(2 Pt 2) (1995) H571-82.
[14] G. Sommer, D.C. Haspinger, M. Andra, M. Sacherer, C. Viertler, P. Regitnig, G.A. Holzapfel, Quantification of Shear Deformations and Corresponding Stresses in the Biaxially Tested Human Myocardium, Ann Biomed Eng (2015).
[15] M.B. Furtado, H.T. Nim, S.E. Boyd, N.A. Rosenthal, View from the heart: cardiac fibroblasts in development, scarring and regeneration, Development 143(3) (2016) 387-97.
[16] D.T. Vu, E.C. Martinez, T. Kofidis, Myocardial restoration: is it the cell or the architecture or both?, Cardiol Res Pract 2012 (2012) 240497.
[17] Biomaterials for Cardiac Regeneration, in: E.J. Suuronen, M. Ruel (Eds.) Springer International Publishing, Switzerland, 2015.
[18] K.E. Porter, N.A. Turner, Cardiac fibroblasts: At the heart of myocardial remodeling, Pharmacol Therapeut 123(2) (2009) 255-278.
[19] H. Jawad, N.N. Ali, A.R. Lyon, Q.Z. Chen, S.E. Harding, A.R. Boccaccini, Myocardial tissue engineering: a review, J Tissue Eng Regen Med 1(5) (2007) 327-42.
[20] S.A. Clarke, W.J. Richardson, J.W. Holmes, Modifying the mechanics of healing infarcts: Is better the enemy of good?, J Mol Cell Cardiol 93 (2016) 115-24.
[21] J.W. Holmes, T.K. Borg, J.W. Covell, Structure and mechanics of healing myocardial infarcts, Annu Rev Biomed Eng 7 (2005) 223-53.
[22] M. Di Donato, S. Castelvecchio, L. Menicanti, Surgical treatment of ischemic heart failure: the Dor procedure, Circ J 73 Suppl A (2009) A1-5.
[23] R.H. Jones, E.J. Velazquez, R.E. Michler, G. Sopko, J.K. Oh, C.M. O'Connor, J.A. Hill, L. Menicanti, Z. Sadowski, P. Desvigne-Nickens, J.L. Rouleau, K.L. Lee, S.H. Investigators, Coronary bypass surgery with or without surgical ventricular reconstruction, N Engl J Med 360(17) (2009) 1705-17.
[24] L. Iop, T. Palmosi, E. Dal Sasso, G. Gerosa, Bioengineered tissue solutions for repair, correction and reconstruction in cardiovascular surgery, J Thorac Dis 10(Suppl 20) (2018) S2390-S2411.
[25] Cor PATCH, 2019. cormatrix.com/corpatch.
[26] M.T. Lam, J.C. Wu, Biomaterial applications in cardiovascular tissue repair and regeneration, Expert Rev Cardiovasc Ther 10(8) (2012) 1039-49.
[27] O.H. Haverich A., Maatz W., Borst H.G., Histopathological Evaluation of Woven and Knitted Dacron Grafts for Right Ventricular Conduits: A Comparative Expeh-ental Study, The Annals of Thoracic Surgery 37(5) (1984) 404-411.

[28] W.J. Ehler, J.H. Cissik, V.C. Smith, G.B. Hubbard, Evaluation of Gore-Tex graft material in the repair of right ventricular outflow tract defect, J Invest Surg 3(2) (1990) 119-27.
[29] S.F. Badylak, P.V. Kochupura, I.S. Cohen, S.V. Doronin, A.E. Saltman, T.W. Gilbert, D.J. Kelly, R.A. Ignotz, G.R. Gaudette, The use of extracellular matrix as an inductive scaffold for the partial replacement of functional myocardium, Cell Transplant 15 (2006) S29-S40.
[30] D. Tang, C. Yang, T. Geva, G. Gaudette, P.J. Del Nido, Multi-Physics MRI-Based Two-Layer Fluid-Structure Interaction Anisotropic Models of Human Right and Left Ventricles with Different Patch Materials: Cardiac Function Assessment and Mechanical Stress Analysis, Comput Struct 89(11-12) (2011) 1059-1068.
[31] M. Banovic, M. Pusnik-Vrckovnik, E. Nakou, P. Vardas, Myocardial regeneration therapy in heart failure: Current status and future therapeutic implications in clinical practice, Int J Cardiol 260 (2018) 124-130.
[32] M. Radisic, K.L. Christman, Materials science and tissue engineering: repairing the heart, Mayo Clin Proc 88(8) (2013) 884-98.
[33] S. Ishigami, S. Ohtsuki, T. Eitoku, D. Ousaka, M. Kondo, Y. Kurita, K. Hirai, Y. Fukushima, K. Baba, T. Goto, N. Horio, J. Kobayashi, Y. Kuroko, Y. Kotani, S. Arai, T. Iwasaki, S. Sato, S. Kasahara, S. Sano, H. Oh, Intracoronary Cardiac Progenitor Cells in Single Ventricle Physiology: The PERSEUS (Cardiac Progenitor Cell Infusion to Treat Univentricular Heart Disease) Randomized Phase 2 Trial, Circ Res 120(7) (2017) 1162-1173.
[34] A. Mozid, C. Yeo, S. Arnous, E. Ako, N. Saunders, D. Locca, P. Brookman, R.A. Archbold, M. Rothman, P. Mills, S. Agrawal, J. Martin, A. Mathur, Safety and feasibility of intramyocardial versus intracoronary delivery of autologous cell therapy in advanced heart failure: the REGENERATE-IHD pilot study, Regen Med 9(3) (2014) 269-78.
[35] J. Kandala, G.A. Upadhyay, E. Pokushalov, S. Wu, D.E. Drachman, J.P. Singh, Meta-analysis of stem cell therapy in chronic ischemic cardiomyopathy, Am J Cardiol 112(2) (2013) 217-25.
[36] M. Wysoczynki, A. Khan, R. Bolli, New Paradigms in Cell Therapy: Repeated Dosing, Intravenous Delivery, Immunomodulatory Actions, and New Cell Types, Circulation Research 123(2) (2018) 138-158.
[37] J. Butler, S.E. Epstein, S.J. Greene, A.A. Quyyumi, S. Sikora, R.J. Kim, A.S. Anderson, J.E. Wilcox, N.I. Tankovich, M.J. Lipinski, Y.A. Ko, K.B. Margulies, R.T. Cole, H.A. Skopicki, M. Gheorghiade, Intravenous Allogeneic Mesenchymal Stem Cells for Nonischemic Cardiomyopathy Safety and Efficacy Results of a Phase II-A Randomized Trial, Circulation Research 120(2) (2017) 332-+.
[38] J. Bartolucci, F.J. Verdugo, P.L. Gonzalez, R.E. Larrea, E. Abarzua, C. Goset, P. Rojo, I. Palma, R. Lamich, P.A. Pedreros, G. Valdivia, V.M. Lopez, C. Nazzal, F. Alcayaga-Miranda, J. Cuenca, M.J. Brobeck, A.N. Patel, F.E. Figueroa, M. Khoury, Safety and Efficacy of the Intravenous Infusion of Umbilical Cord Mesenchymal Stem Cells in Patients

With Heart Failure A Phase 1/2 Randomized Controlled Trial (RIMECARD Trial [Randomized Clinical Trial of Intravenous Infusion Umbilical Cord Mesenchymal Stem Cells on Cardiopathy]), Circulation Research 121(10) (2017) 1192-+.
[39] K.J. Hansen, J.T. Favreau, J.P. Guyette, Z.W. Tao, S.T. Coffin, A. Cunha-Gavidia, B. D'Amore, L.R. Perreault, J.P. Fitzpatrick, A. DeMartino, G.R. Gaudette, Functional Effects of Delivering Human Mesenchymal Stem Cell-Seeded Biological Sutures to an Infarcted Heart, Bioresearch Open Acc 5(1) (2016) 249-260.
[40] Z.W. Tao, J.T. Favreau, J.P. Guyette, K.J. Hansen, J. Lessard, E. Burford, G.D. Pins, G.R. Gaudette, Delivering stem cells to the healthy heart on biological sutures: effects on regional mechanical function, J Tissue Eng Regen Med (2014).
[41] J.P. Guyette, M. Fakharzadeh, E.J. Burford, Z.W. Tao, G.D. Pins, M.W. Rolle, G.R. Gaudette, A novel suture-based method for efficient transplantation of stem cells, J Biomed Mater Res A 101(3) (2013) 809-18.
[42] M.A. Laflamme, C.E. Murry, Heart regeneration, Nature 473(7347) (2011) 326-35.
[43] L. Warren, P.D. Manos, T. Ahfeldt, Y.H. Loh, H. Li, F. Lau, W. Ebina, P.K. Mandal, Z.D. Smith, A. Meissner, G.Q. Daley, A.S. Brack, J.J. Collins, C. Cowan, T.M. Schlaeger, D.J. Rossi, Highly efficient reprogramming to pluripotency and directed differentiation of human cells with synthetic modified mRNA, Cell Stem Cell 7(5) (2010) 618-30.
[44] J. Nussbaum, E. Minami, M.A. Laflamme, J.A. Virag, C.B. Ware, A. Masino, V. Muskheli, L. Pabon, H. Reinecke, C.E. Murry, Transplantation of undifferentiated murine embryonic stem cells in the heart: teratoma formation and immune response, FASEB J 21(7) (2007) 1345-57.
[45] W. Dhahri, R. Romagnuolo, M.A. Laflamme, Training heart tissue to mature, Nat Biomed Eng 2(6) (2018) 351-352.
[46] Y. Shiba, T. Gomibuchi, T. Seto, Y. Wada, H. Ichimura, Y. Tanaka, T. Ogasawara, K. Okada, N. Shiba, K. Sakamoto, D. Ido, T. Shiina, M. Ohkura, J. Nakai, N. Uno, Y. Kazuki, M. Oshimura, I. Minami, U. Ikeda, Allogeneic transplantation of iPS cell-derived cardiomyocytes regenerates primate hearts, Nature 538(7625) (2016) 388-+.
[47] E. Abdelwahid, A. Kalvelyte, A. Stulpinas, K.A. de Carvalho, L.C. Guarita-Souza, G. Foldes, Stem cell death and survival in heart regeneration and repair, Apoptosis 21(3) (2016) 252-68.
[48] X. Li, K. Tamama, X. Xie, J. Guan, Improving Cell Engraftment in Cardiac Stem Cell Therapy, Stem Cells Int 2016 (2016) 7168797.
[49] J. Bartunek, W. Sherman, M. Vanderheyden, F. Fernandez-Aviles, W. Wijns, A. Terzic, Delivery of biologics in cardiovascular regenerative medicine, Clin Pharmacol Ther 85(5) (2009) 548-52.
[50] K.L. Coulombe, V.K. Bajpai, S.T. Andreadis, C.E. Murry, Heart Regeneration with Engineered Myocardial Tissue, Annu Rev Biomed Eng (2014).
[51] L.A. Reis, L.L. Chiu, N. Feric, L. Fu, M. Radisic, Biomaterials in myocardial tissue engineering, J Tissue Eng Regen Med 10(1) (2014) 11-28.

[52] N.J. Kaiser, K.L. Coulombe, Physiologically inspired cardiac scaffolds for tailored in vivo function and heart regeneration, Biomed Mater 10(3) (2015) 034003.
[53] A.M. Shum, H. Che, A.O. Wong, C. Zhang, H. Wu, C.W. Chan, K. Costa, M. Khine, C.W. Kong, R.A. Li, A Micropatterned Human Pluripotent Stem Cell-Based Ventricular Cardiac Anisotropic Sheet for Visualizing Drug-Induced Arrhythmogenicity, Adv Mater 29(1) (2017).
[54] S. Rangarajan, L. Madden, N. Bursac, Use of Flow, Electrical, and Mechanical Stimulation to Promote Engineering of Striated Muscles, Ann Biomed Eng 42(7) (2014) 1391-1405.
[55] G.C. Engelmayr, Jr., M. Cheng, C.J. Bettinger, J.T. Borenstein, R. Langer, L.E. Freed, Accordion-like honeycombs for tissue engineering of cardiac anisotropy, Nat Mater 7(12) (2008) 1003-10.
[56] W. Bian, C.P. Jackman, N. Bursac, Controlling the structural and functional anisotropy of engineered cardiac tissues, Biofabrication 6(2) (2014) 024109.
[57] F. Munarin, N.J. Kaiser, T.Y. Kim, B.R. Choi, K.L.K. Coulombe, Laser-Etched Designs for Molding Hydrogel-Based Engineered Tissues, Tissue Eng Part C Methods 23(5) (2017) 311-321.
[58] W. Bian, B. Liau, N. Badie, N. Bursac, Mesoscopic hydrogel molding to control the 3D geometry of bioartificial muscle tissues, Nat Protoc 4(10) (2009) 1522-34.
[59] Y. Ito, Surface micropatterning to regulate cell functions, Biomaterials 20(23-24) (1999) 2333-42.
[60] T.C. McDevitt, J.C. Angello, M.L. Whitney, H. Reinecke, S.D. Hauschka, C.E. Murry, P.S. Stayton, In vitro generation of differentiated cardiac myofibers on micropatterned laminin surfaces, J Biomed Mater Res 60(3) (2002) 472-9.
[61] T. Pong, W.J. Adams, M.A. Bray, A.W. Feinberg, S.P. Sheehy, A.A. Werdich, K.K. Parker, Hierarchical architecture influences calcium dynamics in engineered cardiac muscle, Exp Biol Med (Maywood) 236(3) (2011) 366-73.
[62] S.S. Zhang, S. Hong, A.G. Kleber, L.P. Lee, R.M. Shaw, A micropatterning approach for imaging dynamic Cx43 trafficking to cell-cell borders, FEBS Lett 588(8) (2014) 1439-45.
[63] M.R. Salick, B.N. Napiwocki, J. Sha, G.T. Knight, S.A. Chindhy, T.J. Kamp, R.S. Ashton, W.C. Crone, Micropattern width dependent sarcomere development in human ESC-derived cardiomyocytes, Biomaterials 35(15) (2014) 4454-64.
[64] L. Yin, H. Bien, E. Entcheva, Scaffold topography alters intracellular calcium dynamics in cultured cardiomyocyte networks, Am J Physiol Heart Circ Physiol 287(3) (2004) H1276-85.
[65] D. Motlagh, T.J. Hartman, T.A. Desai, B. Russell, Microfabricated grooves recapitulate neonatal myocyte connexin43 and N-cadherin expression and localization, J Biomed Mater Res A 67(1) (2003) 148-57.
[66] J. Wang, A. Chen, D.K. Lieu, I. Karakikes, G. Chen, W. Keung, C.W. Chan, R.J. Hajjar, K.D. Costa, M. Khine, R.A. Li, Effect of engineered anisotropy on the susceptibility of

human pluripotent stem cell-derived ventricular cardiomyocytes to arrhythmias, Biomaterials 34(35) (2013) 8878-86.
[67] K.M. Tsang, N. Annabi, F. Ercole, K. Zhou, D. Karst, F. Li, J.M. Haynes, R.A. Evans, H. Thissen, A. Khademhosseini, J.S. Forsythe, Facile One-step Micropatterning Using Photodegradable Methacrylated Gelatin Hydrogels for Improved Cardiomyocyte Organization and Alignment, Adv Funct Mater 25(6) (2015) 977-986.
[68] A.S.T. Smith, H. Yoo, H. Yi, E.H. Ahn, J.H. Lee, G.Z. Shao, E. Nagornyak, M.A. Laflamme, C.E. Murry, D.H. Kim, Micro- and nano-patterned conductive graphene-PEG hybrid scaffolds for cardiac tissue engineering, Chem Commun 53(53) (2017) 7412-7415.
[69] K. Chen, A. Vigliotti, M. Bacca, R.M. McMeeking, V.S. Deshpande, J.W. Holmes, Role of boundary conditions in determining cell alignment in response to stretch, P Natl Acad Sci USA 115(5) (2018) 986-991.
[70] H.T.H. Au, I. Cheng, M.F. Chowdhury, M. Radisic, Interactive effects of surface topography and pulsatile electrical field stimulation on orientation and elongation of fibroblasts and cardiomyocytes, Biomaterials 28(29) (2007) 4277-4293.
[71] J.L. Ruan, N.L. Tulloch, M.V. Razumova, M. Saiget, V. Muskheli, L. Pabon, H. Reinecke, M. Regnier, C.E. Murry, Mechanical Stress Conditioning and Electrical Stimulation Promote Contractility and Force Maturation of Induced Pluripotent Stem Cell-Derived Human Cardiac Tissue, Circulation 134(20) (2016) 1557-1567.
[72] H.T. Au, I. Cheng, M.F. Chowdhury, M. Radisic, Interactive effects of surface topography and pulsatile electrical field stimulation on orientation and elongation of fibroblasts and cardiomyocytes, Biomaterials 28(29) (2007) 4277-93.
[73] The Immune Response to Implanted Materials and Devices, in: B. Corradetti (Ed.) The Impact of the Immune System on the Success of an Implant, Springer International Publishing, Switzerland, 2017.
[74] N.F. Huang, V. Serpooshan, V.B. Morris, N. Sayed, G. Pardon, O.J. Abilez, K.H. Nakayama, B.L. Pruitt, S.M. Wu, Y.S. Yoon, J. Zhang, J.C. Wu, Big bottlenecks in cardiovascular tissue engineering, Commun Biol 1 (2018) 199.
[75] Y. Shiba, D. Filice, S. Fernandes, E. Minami, S.K. Dupras, B.V. Biber, P. Trinh, Y. Hirota, J.D. Gold, M. Viswanathan, M.A. Laflamme, Electrical Integration of Human Embryonic Stem Cell-Derived Cardiomyocytes in a Guinea Pig Chronic Infarct Model, J Cardiovasc Pharmacol Ther 19(4) (2014) 368-381.
[76] J.J. Chong, X. Yang, C.W. Don, E. Minami, Y.W. Liu, J.J. Weyers, W.M. Mahoney, B. Van Biber, S.M. Cook, N.J. Palpant, J.A. Gantz, J.A. Fugate, V. Muskheli, G.M. Gough, K.W. Vogel, C.A. Astley, C.E. Hotchkiss, A. Baldessari, L. Pabon, H. Reinecke, E.A. Gill, V. Nelson, H.P. Kiem, M.A. Laflamme, C.E. Murry, Human embryonic-stem-cell-derived cardiomyocytes regenerate non-human primate hearts, Nature 510(7504) (2014) 273-7.
[77] S.S. Nunes, J.W. Miklas, J. Liu, R. Aschar-Sobbi, Y. Xiao, B. Zhang, J. Jiang, S. Masse, M. Gagliardi, A. Hsieh, N. Thavandiran, M.A. Laflamme, K. Nanthakumar, G.J. Gross, P.H.

Backx, G. Keller, M. Radisic, Biowire: a platform for maturation of human pluripotent stem cell-derived cardiomyocytes, Nat Methods 10(8) (2013) 781-7.
[78] M.O. Chrobak, K.J. Hansen, J.R. Gershlak, M. Vratsanos, M. Kanellias, G.R. Gaudette, G.D. Pins, Design of a fibrin microthread-based composite layer for use in a cardiac patch, ACS Biomaterials Science & Engineering (2016).
[79] T.A. Ahmed, E.V. Dare, M. Hincke, Fibrin: a versatile scaffold for tissue engineering applications, Tissue Eng Part B Rev 14(2) (2008) 199-215.
[80] S. Hinds, W. Bian, R.G. Dennis, N. Bursac, The role of extracellular matrix composition in structure and function of bioengineered skeletal muscle, Biomaterials 32(14) (2011) 3575-83.
[81] J.M. Grasman, D.M. Do, R.L. Page, G.D. Pins, Rapid release of growth factors regenerates force output in volumetric muscle loss injuries, Biomaterials 72 (2015) 49-60.
[82] Z.W. Tao, M. Mohamed, M. Hogan, L. Gutierrez, R.K. Birla, Optimizing a spontaneously contracting heart tissue patch with rat neonatal cardiac cells on fibrin gel, J Tissue Eng Regen M 11(1) (2017) 153-163.
[83] iCell Cardiomyocytes2, 2019. fujifilmcdi.com/products-services/icell-products/icell-cardiomyocytes2/.
[84] C-Pace System, 2019. ionoptix.com/product/cell-culture-pacing/.
[85] K.A. Bush, G.D. Pins, Development of Microfabricated Dermal Epidermal Regenerative Matrices to Evaluate the Role of Cellular Microenvironments on Epidermal Morphogenesis, Tissue Eng Pt A 18(21-22) (2012) 2343-2353.
[86] M.O. Chrobak, Designing Modular Fibrin Composite Scaffolds for Enhanced Ventricular Myocardium Regeneration, Biomedical Engineering, Worcester Polytechnic Institute, Worcster, MA, 2017, p. 170.
[87] K.J. Hansen, J.T. Favreau, J.R. Gershlak, M.A. Laflamme, D.R. Albrecht, G.R. Gaudette, Optical Method to Quantify Mechanical Contraction and Calcium Transients of Human Pluripotent Stem Cell-Derived Cardiomyocytes, Tissue Eng Part C Methods (2017).
[88] D.J. Kelly, E.U. Azeloglu, P.V. Kochupura, G.S. Sharma, G.R. Gaudette, Accuracy and reproducibility of a subpixel extended phase correlation method to determine micron level displacements in the heart, Med Eng Phys 29(1) (2007) 154-62.
[89] Photomasks and Phototools, 2017. outputcity.com.
[90] A. Tijore, S.A. Irvine, U. Sarig, P. Mhaisalkar, V. Baisane, S. Venkatraman, Contact guidance for cardiac tissue engineering using 3D bioprinted gelatin patterned hydrogel, Biofabrication 10(2) (2018).
[91] A.E. Zemljic-Harpf, J.C. Godoy, O. Platoshyn, E.K. Asfaw, A.R. Busija, A.A. Domenighetti, R.S. Ross, Vinculin directly binds zonula occludens-1 and is essential for stabilizing connexin-43-containing gap junctions in cardiac myocytes, J Cell Sci 127(5) (2014) 1104-1116.

[92] M.T. Lam, S. Sim, X.Y. Zhu, S. Takayama, The effect of continuous wavy micropatterns on silicone substrates on the alignment of skeletal muscle myoblasts and myotubes, Biomaterials 27(24) (2006) 4340-4347.
[93] K. Nagamine, T. Kawashima, T. Ishibashi, H. Kaji, M. Kanzaki, M. Nishizawa, Micropatterning Contractile C2C12 Myotubes Embedded in a Fibrin Gel, Biotechnol Bioeng 105(6) (2010) 1161-1167.
[94] J. Iturri, J.L. Toca-Herrera, Characterization of Cell Scaffolds by Atomic Force Microscopy, Polymers-Basel 9(8) (2017).
[95] A. Jiao, C.T. Moerk, N. Penland, M. Perla, J. Kim, A.S.T. Smith, C.E. Murry, D.H. Kim, Regulation of skeletal myotube formation and alignment by nanotopographically controlled cell-secreted extracellular matrix, J Biomed Mater Res A 106(6) (2018) 1543-1551.
[96] N.F. Huang, R.J. Lee, S. Li, Engineering of aligned skeletal muscle by micropatterning, Am J Transl Res 2(1) (2010) 43-55.
[97] M.O. Chrobak, E.J. English, M. Kanellias, K.J. Hansena, J.R. Gershlak, G.R. Gaudette, G.D. Pins, Anisotropic Tension Increases Cardiomyocyte Alignment and Contractile Strain in Composite Fibrin Scaffolds In Preparation. (2019).
[98] C. Robertson, D.D. Tran, S.C. George, Concise review: maturation phases of human pluripotent stem cell-derived cardiomyocytes, Stem Cells 31(5) (2013) 829-37.
[99] S.M. LoRusso, D. Rhee, J.M. Sanger, J.W. Sanger, Premyofibrils in spreading adult cardiomyocytes in tissue culture: evidence for reexpression of the embryonic program for myofibrillogenesis in adult cells, Cell Motil Cytoskeleton 37(3) (1997) 183-98.
[100] C.D. Merkel, Y. Li, Q. Raza, D.B. Stolz, A.V. Kwiatkowski, Vinculin anchors contractile actin to the cardiomyocyte adherens junction, Mol Biol Cell 30(21) (2019) 2639-2650.
[101] R. Santoro, G.L. Perrucci, A. Gowran, G. Pompilio, Unchain My Heart: Integrins at the Basis of iPSC Cardiomyocyte Differentiation, Stem Cells Int (2019).
[102] H. Duong, B. Wu, B. Tawil, Modulation of 3D fibrin matrix stiffness by intrinsic fibrinogen-thrombin compositions and by extrinsic cellular activity, Tissue Eng Part A 15(7) (2009) 1865-76.
[103] I. Karakikes, M. Ameen, V. Termglinchan, J.C. Wu, Human Induced Pluripotent Stem Cell-Derived Cardiomyocytes Insights Into Molecular, Cellular, and Functional Phenotypes, Circulation Research 117(1) (2015) 80-88.
[104] W.L. Stoppel, D.L. Kaplan, L.D. Black, 3rd, Electrical and mechanical stimulation of cardiac cells and tissue constructs, Adv Drug Deliv Rev 96 (2016) 135-55.
[105] K. Ronaldson-Bouchard, K. Yeager, D. Teles, T. Chen, S. Ma, L. Song, K. Morikawa, H.M. Wobma, A. Vasciaveo, E.C. Ruiz, M. Yazawa, G. Vunjak-Novakovic, Engineering of human cardiac muscle electromechanically matured to an adult-like phenotype, Nat Protoc 14(10) (2019) 2781-2817.

[106] L.L.Y. Chiu, R.K. Iyer, J.P. King, M. Radisic, Biphasic Electrical Field Stimulation Aids in Tissue Engineering of Multicell-Type Cardiac Organoids, Tissue Eng Pt A 17(11-12) (2011) 1465-1477.
[107] C.C. Moore, C.H. Lugo-Olivieri, E.R. McVeigh, E.A. Zerhouni, Three-dimensional systolic strain patterns in the normal human left ventricle: characterization with tagged MR imaging, Radiology 214(2) (2000) 453-66.
[108] N.R. Clark, N. Reichek, P. Bergey, E.A. Hoffman, D. Brownson, L. Palmon, L. Axel, Circumferential myocardial shortening in the normal human left ventricle. Assessment by magnetic resonance imaging using spatial modulation of magnetization, Circulation 84(1) (1991) 67-74.
[109] K.J. Hansen, M.A. Laflamme, G.R. Gaudette, Development of a Contractile Cardiac Fiber From Pluripotent Stem Cell Derived Cardiomyocytes, Front Cardiovasc Med 5 (2018) 52.
[110] L. Madden, M. Juhas, W.E. Kraus, G.A. Truskey, N. Bursac, Bioengineered human myobundles mimic clinical responses of skeletal muscle to drugs, Elife 4 (2015) e04885.
[111] A.K. Capulli, L.A. MacQueen, S.P. Sheehy, K.K. Parker, Fibrous scaffolds for building hearts and heart parts, Adv Drug Deliv Rev 96 (2016) 83-102.
[112] C. Kane, C.M. Terracciano, Cardiac Fibroblast Co-Culture Promotes More Adult- Like Electrophysiological Properties in Human Induced Pluripotent Stem Cell-Derived Cardiomyocytes, Circulation 134 (2016).
[113] J.R. Gershlak, S. Hernandez, G. Fontana, L.R. Perreault, K.J. Hansen, S.A. Larson, B.Y.K. Binder, D.M. Dolivo, T.H. Yang, T. Dominko, M.W. Rolle, P.J. Weathers, F. Medina-Bolivar, C.L. Cramer, W.L. Murphy, G.R. Gaudette, Crossing kingdoms: Using decellularized plants as perfusable tissue engineering scaffolds, Biomaterials 125 (2017) 13-22.
[114] J.E. Santos, Towards the Fabrication of a Fibrin Based Vascular Network, Biomedical Engineering, Worcester Polytechnic Institute, Worcester, MA, 2018.
[115] D. Cerkanowicz, M. Conlen, S. Ghahremani, A. Rosenthal, Design of a Biomimetic Mechanical Stimulator for Engineered Myocardium, Biomedical Engineering, Worcester Polytechnic Institute, Worcester, MA, 2019.
[116] J.G. Jacot, A.D. McCulloch, J.H. Omens, Substrate stiffness affects the functional maturation of neonatal rat ventricular myocytes, Biophys J 95(7) (2008) 3479-87.
[117] A.J. Engler, C. Carag-Krieger, C.P. Johnson, M. Raab, H.Y. Tang, D.W. Speicher, J.W. Sanger, J.M. Sanger, D.E. Discher, Embryonic cardiomyocytes beat best on a matrix with heart-like elasticity: scar-like rigidity inhibits beating, J Cell Sci 121(Pt 22) (2008) 3794-802.
[118] P. Pandey, W. Hawkes, J.Q. Hu, W.V. Megone, J. Gautrot, N. Anilkumar, M. Zhang, L. Hirvonen, S. Cox, E. Ehler, J. Hone, M. Sheetz, T. Iskratsch, Cardiomyocytes Sense Matrix Rigidity through a Combination of Muscle and Non-muscle Myosin Contractions (vol 44, pg 326, 2018), Developmental Cell 45(5) (2018) 661-661.

Appendix A

Photolithography mask (A) and magnified micropatterns (B) used to create the micropatterned silicon wafer. The mask was designed to have five micropatterns of the same geometries in order to allow multiple PDMS negative replicates to be produced from the silicon wafer.

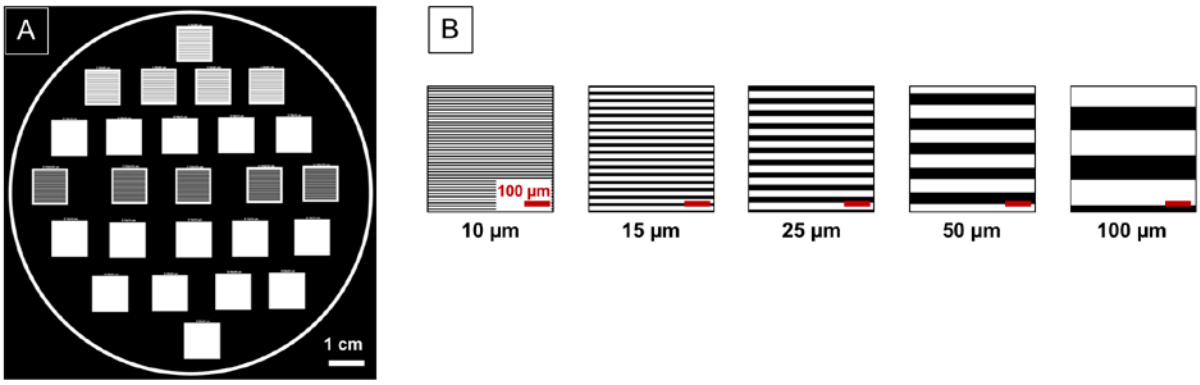

Figure 26 Photolithography mask (A) and magnified micropatterns (B) used to create the patterned silicon wafer.

Appendix B

Phase images of hiPS-CM seeded 0 µm hydrogels on days 2, 3, 7, and 14. Nuclear alignment experiments were performed on cells seeded for 7 days. As per manufacturer recommendations and images provided by customer service, CDI's iCell Cardiomyocyte^2 are fully adhered and elongated between 5-7 days post-thaw [83]. As can be seen here, cells are attached and beginning to spread out on Days 2 and 3. By Day 7, all cells are fully spread out and oriented on unpatterned hydrogels.

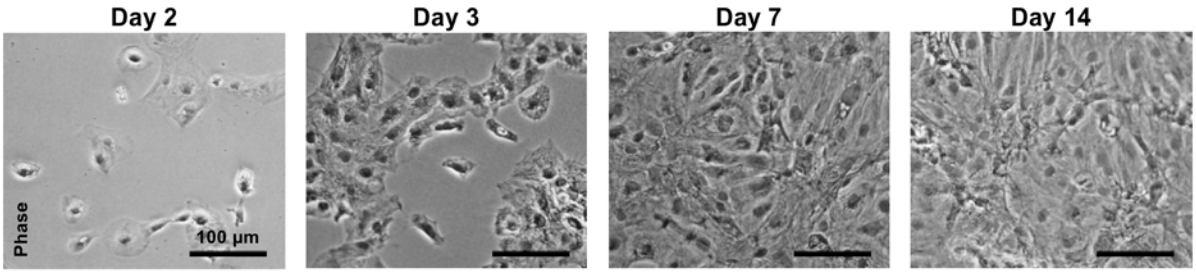

Figure 27 Phase images of hiPS-CM seeded 0 µm hydrogels on days 2, 3, 7, and 14.

Appendix C

Micropatterned fibrin hydrogels with incorporated fibrin microthreads were cryosectioned to show orthogonal view of the micropattern geometry and thread incorporation. Hydrogels separated into layers in the fixing and sectioning process, and micropatterns were difficult to visualize due to hydrogel shrinkage during fixation, which can be visualized by the hydrogels pulling away from the threads. Additionally, shrinkage cause the fibrin hydrogel to pull away from incorporated fibrin microthreads. Because visualization was limited and shrinkage occurred, rhodamine coated hydrogels and confocal microscopy were used to measure micropattern geometry.

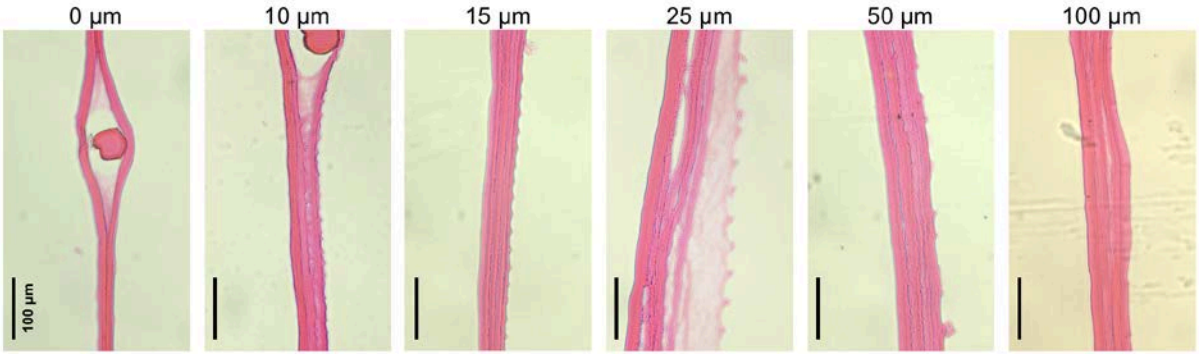

Figure 28 Micropatterned fibrin hydrogels with incorporated fibrin microthreads were cryosectioned to show orthogonal view of the micropattern geometry and thread incorporation. Hydrogels separated into layers in the fixing and sectioning process, and micropatterns were difficult to visualize due to hydrogel shrinkage during fixation. Additionally, shrinkage cause the fibrin hydrogel to pull away from incorporated fibrin microthreads. Because visualization was limited and shrinkage occurred, rhodamine coated hydrogels and confocal microscopy were used to measure micropattern geometry.

Appendix D

Histogram of the distribution of the total number of cells in each binning group for C2C12 alignment.

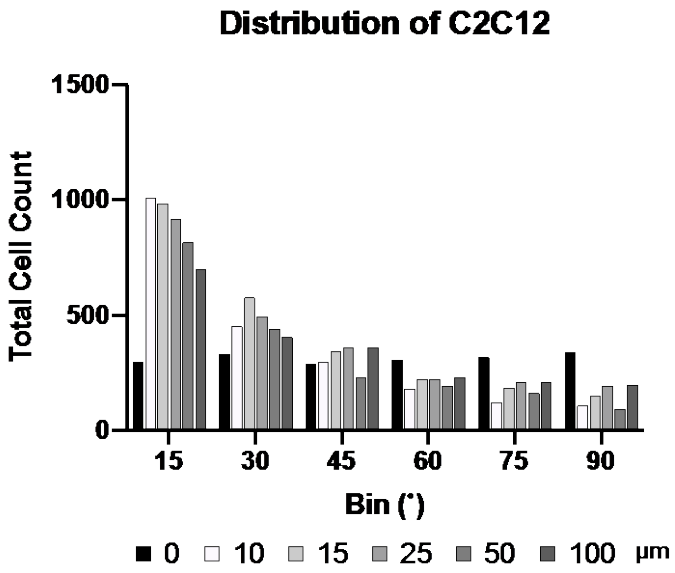

Figure 29 Histogram of the distribution of the total number of cells in each binning group for C2C12 alignment.

Appendix E

Histogram of the distribution of the total number of cells in each binning group for hiPS-CM alignment (A) and hiPS-CM alignment when cultured under C-Pace electrical stimulation (B). Please cross-reference Appendix I for alignment of hiPS-CM under electrical stimulation.

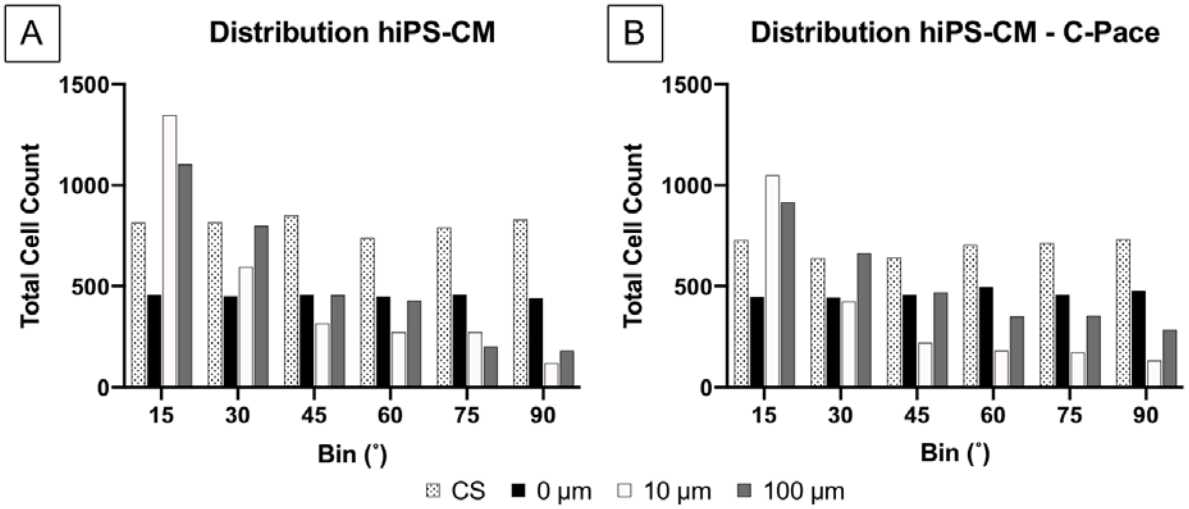

Figure 30 Histogram of the distribution of the total number of cells in each binning group for hiPS-CM alignment (A) and hiPS-CM alignment when cultured under C-Pace electrical stimulation (B).

Appendix F

Negative and positive controls for sarcomeric α-actinin, connexin-43, and Hoechst. Negative control was incubated with secondary antibodies but no primary antibodies, and the positive control was cryosectioned human heart.

Source: Chrobak MO, English EJ,…,Pins GD. “Anisotropic Tension Increases Cardiomyocyte Alignment and Contractile Strain in Composite Fibrin Scaffolds.” 2019. In Submission.

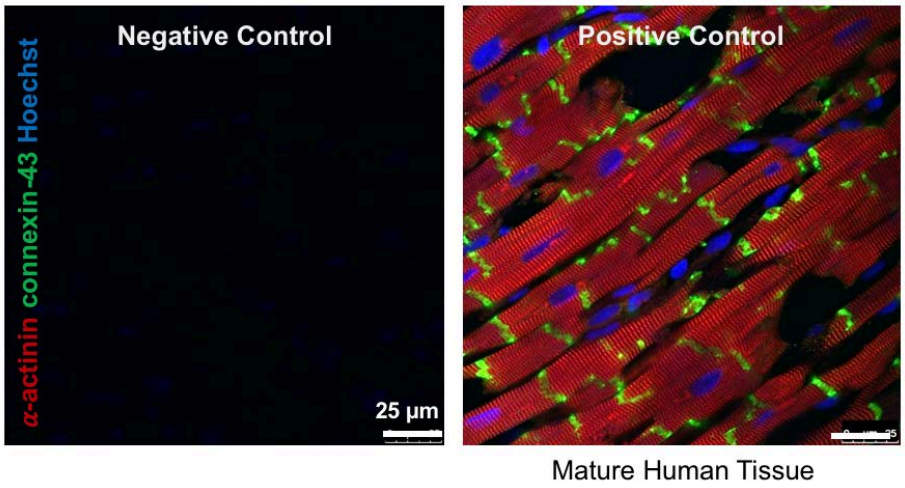

Figure 31 Negative and positive controls for sarcomeric α-actinin, connexin-43, and Hoechst. Negative control was incubated with secondary antibodies but no primary antibodies, and the positive control was cryosectioned human heart.

Source: Chrobak MO, English EJ,…,Pins GD. “Anisotropic Tension Increases Cardiomyocyte Alignment and Contractile Strain in Composite Fibrin Scaffolds.” 2019. In Submission.

Appendix G

Negative control of vinculin antibody. Sample incubated with secondary and no primary antibody.

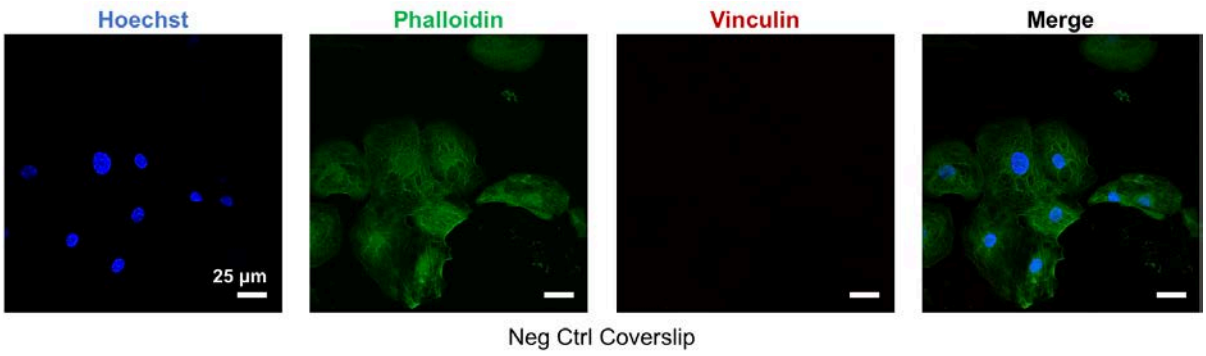

Figure 32 Negative control of vinculin antibody. Sample incubated with secondary and no primary antibody.

Appendix H

Phenotypic analysis of C-Pace cultured hiPS-CM seeded constructs at Day 7 (top) and Day 14 (bottom) in representative images. Dotted lines denote micropattern direction. Please cross-reference Figure 17 for comparison to static cultured constructs.

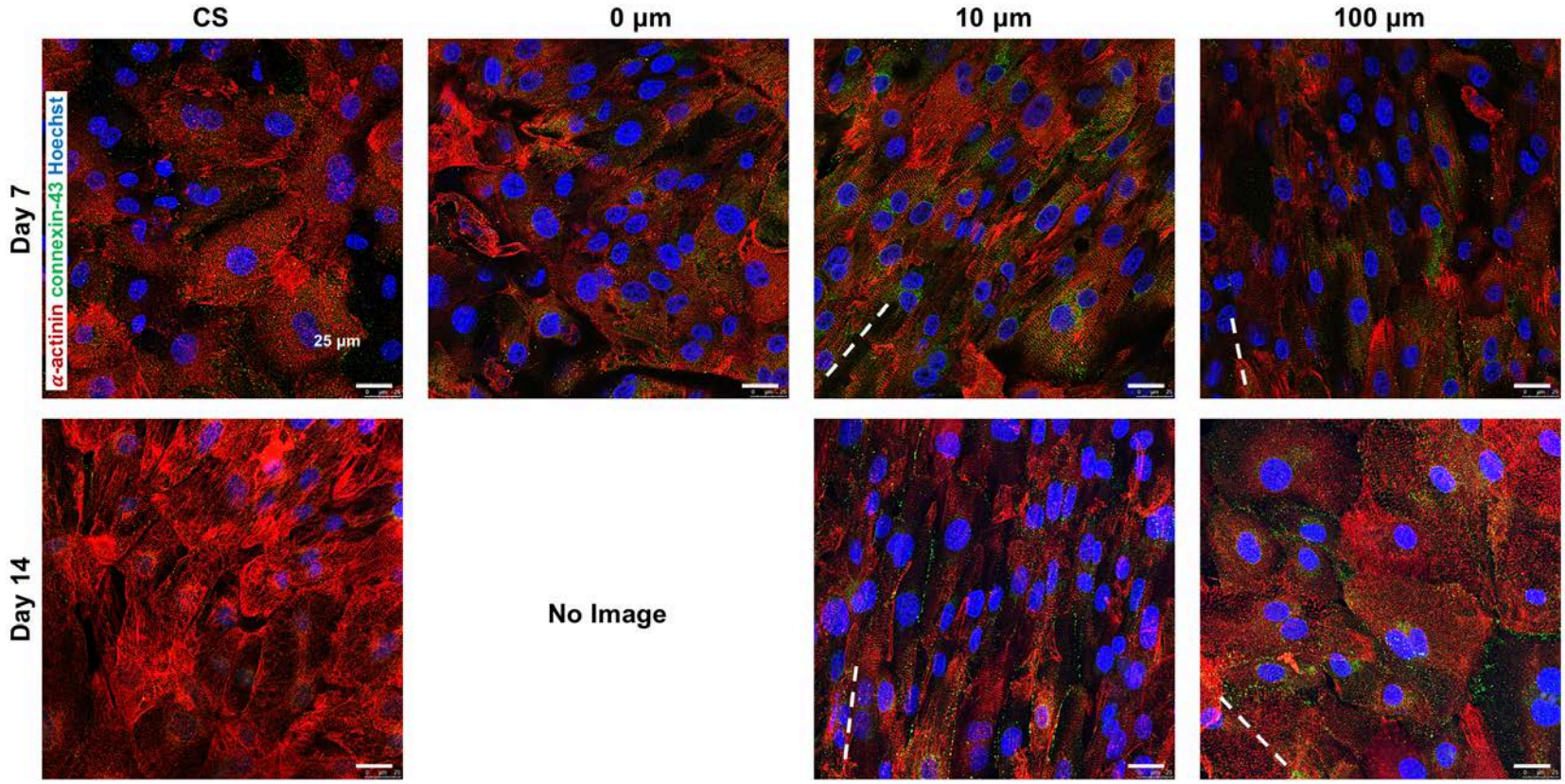

Figure 33 Phenotypic analysis of C-Pace cultured hiPS-CM seeded constructs at Day 7 (top) and Day 14 (bottom) in representative images. Dotted lines denote micropattern direction.

Appendix I

(A) Representative phase and Hoechst images of electrically stimulated coverslips and 0 µm, 10 µm, and 100 µm hydrogels. Dotted lines denote micropattern direction. (B) Percent nuclear alignment and (C) average nuclear angle of hiPS-CM seeded constructs with respect to static and C-Pace culture after 7 days of culture. There were no statistical differences between culture conditions and nuclear alignment. Please cross-reference Figure 16 for comparison to static cultured constructs.

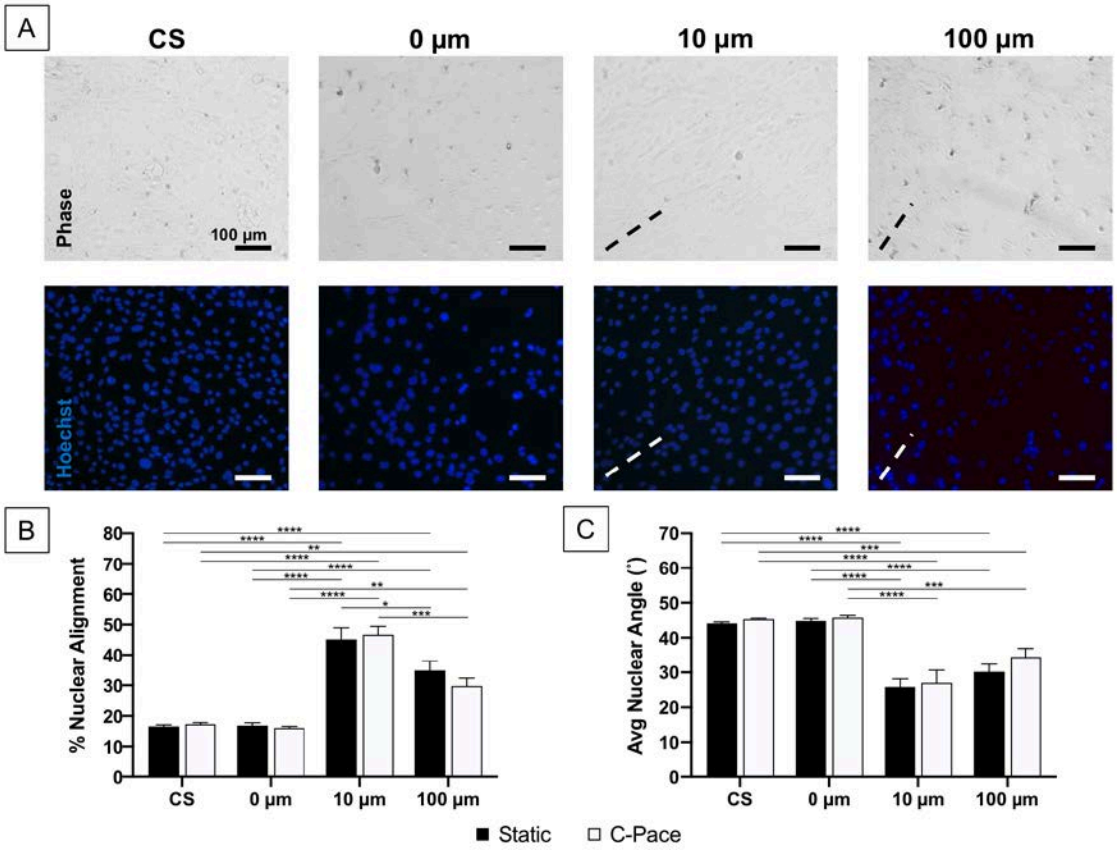

*Figure 34 (A) Representative phase and Hoechst images of hiPS-CM seeded coverslips and 0 µm, 10 µm, and 100 µm hydrogels after 7 days of electrical stimulation culture. Dotted lines denote micropattern direction. (B) Percent alignment of hiPS-CM nuclei with respect to the direction of the micropatterned surface. Alignment is defined as falling within 15˚ of the axis. (C) The average angle of hiPS-CM nuclei was examined, with 0˚ indicating perfect alignment. There were no statistical differences between culture conditions and nuclear alignment. Mean±SEM. Normality was determined with Shapiro-Wilk test, and a Two-way ANOVA with Sidak post-hoc analysis was performed. A bar represents significant difference, p<0.0332 for *, p<0.0021 for **, p<0.0002 for ***, p<0.0001 for ****. N ≥4. ~ 300 cells/image were analyzed.*